SLAC – PUB – 4169
December 1986
(A)

WAKEFIELD EFFECTS IN A LINEAR COLLIDER*

KARL L. F. BANE

Stanford Linear Accelerator Center
Stanford University, Stanford, California, 94305

Contributed to the Proceedings of the U.S. Summer
School on High Energy Particle Accelerators.
Batavia, Illinois, Aug. 13-31, 1984.

⋆ Work supported by the Department of Energy, contracts and DE-AC03-76SF00515.

1. INTRODUCTION

In a linear collider an intense, ultra-relativistic bunched electron (or positron) beam traverses a large number of accelerating cells on its way to the interaction point. Strong wakefields will be excited. The longitudinal wakefields will cause the beam to lose energy and induce an energy spread along the bunch. If the bunch does not move along a symmetry axis of the accelerating structure, transverse wakefields will be excited. The beam can then develop a corkscrew-like tail in a process called single bunch beam break-up. One cause can be static errors along the linac that are not perfectly corrected. Or, if there are errors in the manufacture of the accelerating structure, there may not even be a symmetry axis along which the bunch should move to avoid transverse wakefields. The cause can be jitter (a pulse-to-pulse variation) in injection, or jitter in field quality or component positioning along the linac; if they are random, these errors are probably uncorrectable in a linac. Beam breakup can affect the collider performance in many ways. The tail of the beam will confuse position monitor readings, making it difficult or impossible to correct the orbit. The tail particles themselves, or showers of secondaries that they can create when impinging on an insertion, can damage equipment or confuse the detector. Even when particles are not lost the luminosity can be greatly reduced.

The luminosity of two identical unperturbed beams with gaussian profiles colliding head-on is given by

$$\mathcal{L} = \frac{N^2 f_{rep}}{4\pi\sigma_x\sigma_y} , \tag{1.1}$$

where N is the total number of particles in each bunch, f_{rep} is the repetition rate and σ_x, σ_y give the beam size in the transverse plane. Since $\sigma_x = \sqrt{\epsilon_x\beta_x}$ and similarly for the y plane, with ϵ the emittance and β the beta function, we see that the luminosity varies inversely as the emittance. We will introduce an

effective emittance growth factor in this paper that can be used as a figure of merit for the luminosity reduction, at least for modest emittance growth. Note that Eq. (1.1) does not give the luminosity for a perturbed beam in which case the correct overlap integral can give a very complicated expression.

In this paper we first discuss the wakefields for the SLAC accelerating structure, then some considerations dealing with the longitudinal wakefields. The main focus, though, will be on the effects of the transverse wakefield on the beam, including the case when there is an energy variation along the bunch. The use of an energy spread to inhibit emittance growth in a linac, indeed to damp the oscillations of the core of the bunch to below the unperturbed betatron oscillations, (in a process that is similar to Landau Damping) was first described by Balakin *et. al.*[1] These authors have done quite extensive work on the transverse beam dynamics in colliders (see in particular Ref. 2). Our approach will be more qualitative in nature. In the final chapter the example of the SLC, including errors, will be studied in detail.

The bunch-to-bunch or long range wakefield effects will not be discussed in this paper. The transverse long range wakes can cause an instability also called beam break-up, which should not be confused with the single bunch beam break-up of short bunches discussed in this paper.

2. WAKEFIELDS FOR AN ACCELERATING STRUCTURE

Consider a high intensity, ultra-relativistic bunched electron beam moving in a straight line. If the bunch is moving within a smooth, perfectly conducting pipe there is little electromagnetic interaction between the particles within the bunch; the Lorentz force between the particles is of order γ^{-2}, with γ the beam energy. If, however, the walls have a longitudinally varying shape, as is the case with an RF cavity, or if the smooth pipe has a finite resistivity, this is no longer true. Due to these wall perturbations, the head of the beam excites electromagnetic fields that kick the tail with an intensity that does not diminish as $\gamma \to \infty$. These electromagnetic forces are called wakefields, since from causality the head can kick the tail and not vice versa. They depend linearly on the charge Q of the beam and are only important in high intensity accelerators.

If we integrate the force felt be a co-moving test charge over a cell or over a meter of structure we have the wake potentials. Instead of a quantity that depends on position with respect to the bunch and time we are now left with a function of position only. The integral of the longitudinal electric field gives the longitudinal wake potential, a knowledge of which may be used to find the total energy loss of the bunch as well as its induced energy spread. The integral of the transverse Lorentz force gives the transverse wake potential which is used to study the transverse dynamics of the beam. If the beam is sufficiently

rigid so that changes in its transverse position are negligible over the length of an accelerating cell, the wake potentials can be used as Green's functions in the equation of motion of bunch macro-particles, thus greatly simplifying the problem. On the other hand, the concept of wake potential is of little utility at the low energy end of an accelerator, near the gun. For these problems the electromagnetic fields and the equation of motion of bunch particles must be solved self-consistently.

2.1 Wakefields of a Point Charge

Consider now an ultra-relativistic exciting particle of charge Q moving in the z direction in an accelerating structure of length L. The longitudinal wake potential W_z (more precisely, the delta-function longitudinal wake potential) is defined as the total voltage lost by a test charge following at a distance s on the same path, divided by LQ:

$$W_z(s) = -\frac{1}{LQ}\int_0^L dz\; E_z(z,(z+s)/c) \tag{2.1}$$

where $E_z(z,t)$ is the z component of the electric field $\mathbf{E}$ on the path of traversal. We have set the magnitude of the velocity v to the speed of light c, an approximation which will not change the result significantly for high energy particles. Note that since a signal cannot travel faster than the speed of light, $W_z = 0$ for $s < 0$. Similarly the transverse wake potential $\mathbf{W}_\perp$ is defined as the transverse momentum kick experienced by the test charge divided by LQ. (Note that $\mathbf{W}_\perp$ is a vector with both x and y components.) Thus

$$\mathbf{W}_\perp(s) \;=\; \frac{1}{LQ}\int_0^L dz\; [\mathbf{E}_\perp + (\mathbf{v}\times\mathbf{B})_\perp]_{t=(z+s)/c} \quad . \tag{2.2}$$

We approximate the SLAC linac accelerating structure by a periodic, cylindrically symmetric disk-loaded structure with period p and iris radius a (see Fig. 1b). In a cylindrically symmetric structure all the modes depend on the azimuthal angle θ as $e^{im\theta}$, where m is an integer. The $m = 0, 1, 2$ modes are called respectively the longitudinal, dipole, quadrupole modes. In a periodic structure the modes come in frequency bands, though a charged particle travelling through the structure will only excite a discrete set of these modes. Each mode mn is characterized by a frequency $\omega_{mn}/2\pi$ (the eigenvalue) and a loss factor k_{mn} (the eigenfunction). The loss factors have units of V/pC/m. The possibly more familiar quantity R/Q (the shunt impedance per unit length divided by its quality factor) is simply equal to $4k/\omega$. (For more discussion of this see for example Ref. 3.)

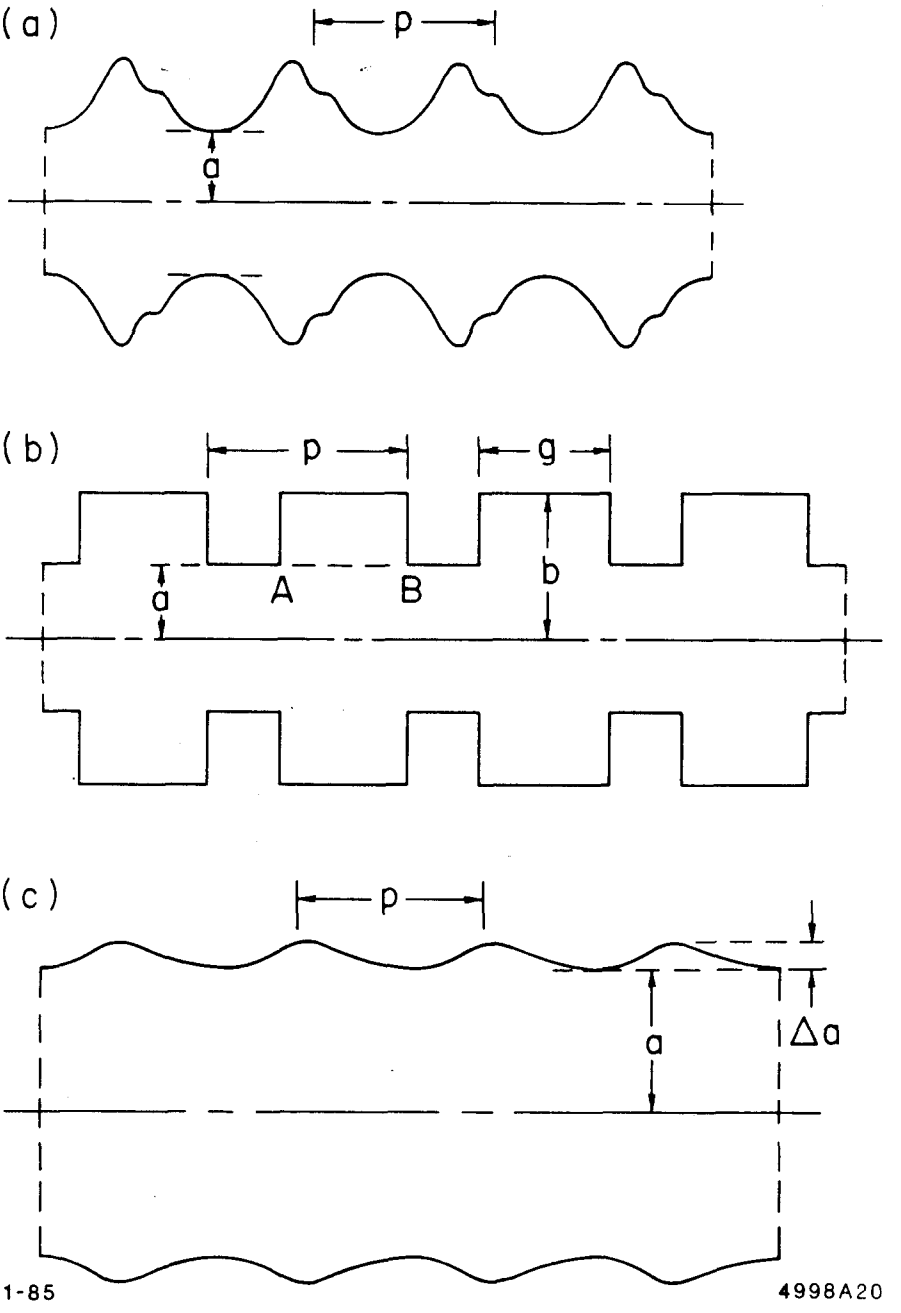

Fig. 1. Examples of cylindrically symmetric periodic structures: (a) general case, (b) all surfaces parallel or perpendicular to the z-axis, (c) weak wall perturbation.

We arrange the axes so that the transverse position of the exciting charge is $r = r'$, $\theta = 0$ (on the x-axis). The test charge also moves in the z direction but at transverse position (r, θ) and at a distance s behind the exciting charge. It can be shown that the m-pole component of the wakes experienced by the test particle can be written as a sum over all the m-pole modes as[3–5]

$$W_{zm} = \left(\frac{r'}{a}\right)^m \left(\frac{r}{a}\right)^m \cos m\theta \sum_n^\infty 2k_{mn} \cos\frac{\omega_{mn}s}{c} \qquad s > 0 \tag{2.3}$$

while for $m \neq 0$

$$\mathbf{W}_{\perp m} = m\left(\frac{r'}{a}\right)^m \left(\frac{r}{a}\right)^{m-1} (\hat{\mathbf{r}}\cos m\theta - \hat{\boldsymbol{\theta}}\sin m\theta) \sum_n^\infty \frac{2k_{mn}}{(\omega_{mn}a/c)} \sin\frac{\omega_{mn}s}{c} \qquad s > 0, \tag{2.4}$$

with $\hat{\mathbf{r}}$, $\hat{\boldsymbol{\theta}}$ the unit vectors in the r and θ directions respectively. For $m = 0$, $\mathbf{W}_{\perp m} = 0$; the longitudinal wakefields do not give a transverse kick. We can summarize the relationship between the components as

$$\frac{\partial}{\partial s}\mathbf{W}_{\perp m} = \nabla_\perp W_{zm} \quad . \tag{2.5}$$

For cylindrically symmetric structures, given one component of the wake potentials the other two are known. Eq. (2.5) is sometimes called the Panofsky-Wenzel Theorem.[6] It applies also to structures that are not cylindrically symmetric.

To get the total wakefield we need to sum over all the multipole contributions excited by the leading charge. Normally bunches remain near the axis and the factors (r/a), (r'/a) can be considered small. Then the longitudinal wakefield is dominated by the longitudinal modes whereas the transverse wakefield is dominated by the dipole modes. Thus normally we can approximate the wakes as

$$W_z \simeq \sum_n^\infty 2k_{0n} \cos\frac{\omega_{0n}s}{c} \qquad s > 0 \tag{2.6}$$

$$\mathbf{W}_\perp \simeq \hat{\mathbf{x}}\left(\frac{r'}{a}\right) \sum_n^\infty \frac{2k_{1n}}{(\omega_{1n}a/c)} \sin\frac{\omega_{1n}s}{c} \qquad s > 0 \quad , \tag{2.7}$$

where $\hat{\mathbf{x}}$ is the unit vector in the x direction. We see that the dependence of the wakefields on transverse position is particularly simple. Note that the longitudinal wake is approximately independent of the transverse position of both the exciting charge and the test charge. The transverse wake depends on the exciting charge as the first power of its offset. The transverse wake is in the x-direction and is independent of the test charge's transverse position.

In this paper we will work in MKS units, with W_z given in units of V/pC/m. To be consistent with common usage we will give the dipole wake W_x in units of V/pC/m^2. That is, we take $\hat{\mathbf{x}} W_x = |\mathbf{W}_\perp|/r'$ with $\mathbf{W}_\perp$ given by Eq. (2.7). To get the transverse kick experienced by the test charge in volts, W_x needs to be multiplied by the charge Q and position r' of the exciting charge, and by the length of the structure L. In Gaussian units W_z is in units of cm^{-2} and W_x in units of cm^{-3}. In these units the scaling of the wakes becomes clear. If all dimensions of the structure are modified by the scaling factor λ then if we also scale s as λ

$$s \sim \lambda \quad , \tag{2.8}$$

we find that the wakes scale as

$$\begin{aligned} W_z &\sim \lambda^{-2} \\ W_x &\sim \lambda^{-3} \end{aligned} \quad . \tag{2.9}$$

Sometimes one is interested in the wake potential of a single cavity with beam tubes. If we take an infinitely repeating structure, increasing the tube length between the cells, we can imagine that the wake potential per cell of the repeating structure will approach the total wake potential for a single cavity with long beam tubes. For proof that Eq. (2.5) as well as the r, θ dependencies of Eqs. (2.3) and (2.4) hold for a single cylindrically symmetric cavity with long beam tubes, see Ref. 7.

2.2 Wakefields of a Charge Distribution

The longitudinal wake of a point charge W_z can be used as a Green's function for computing the voltage loss within an ultra-relativistic bunch of arbitrary shape. When the bunch remains close to the axis of a cylindrically symmetric structure we can solve the longitudinal problem independently of the transverse equation of motion: the voltage induced along the bunch is approximately independent of its transverse position or its transverse shape. This is due to the fact the Green's function W_z is approximately independent of the transverse position of both the exciting charge and the test charge (see Eq. (2.6)). The wakefield induced voltage loss of a test particle at position s within a bunch, per unit total charge Q per meter, will be denoted by $\mathcal{W}_z$. It is also called the wake potential, or sometimes the bunch wake to differentiate it from W_z. The two wakes are connected by

$$\mathcal{W}_z(s) = \frac{1}{Q} \int_0^\infty ds' \; \rho(s - s') \; W_z(s') \quad , \tag{2.10}$$

with $\rho(s)$ the charge distribution of the bunch. Eq. (2.10) is only valid for bunches that remain near the axis of a cylindrically symmetric structure.

A bunch dipole wake $\mathcal{W}_x$ can be defined in a manner analogous to Eq. (2.10). But since the dipole Green's function W_x does depend on the transverse position of the exciting charge (see Eq. (2.7)), $\mathcal{W}_x$ only gives the correct transverse kick within a bunch under the assumption that the bunch is unperturbed and moving at a given offset from the structure axis.

The bunch's total energy loss (per meter of structure) divided by Q^2 is then given by

$$k_{tot} = \frac{1}{Q} \int_{-\infty}^{\infty} ds\ \rho(s) \mathcal{W}_z(s) \quad . \tag{2.11}$$

Combining Eqs. (2.6), (2.10) and (2.11) we find that for a gaussian bunch in a cylindrically symmetric structure the total loss becomes simply

$$k_{tot} \simeq \sum_{n}^{\infty} k_{0n} e^{-(\omega_{0n}\sigma_z/c)^2} \quad . \tag{2.12}$$

The above expression is only approximately true since the higher multipole modes ($m \neq 0$) will also contribute to energy loss. But when the bunch does not stray too far from the structure axis (*i.e.* $(r/a)^2$ is small compared to one, with r the bunch offset) this additional contribution will be small.

Historically the wakefields for the SLAC disk-loaded structure were first calculated by the modal method described here. It should be noted that the wake potentials for a smooth charge distribution can also be calculated by a time domain integration of Maxwell's equations using a computer program such as TBCI.[8] (See also Ref. 9.) This is normally the quickest way of finding the bunch wakes $\mathcal{W}_z$, $\mathcal{W}_x$ of a cylindrically symmetric structure of arbitrary shape. If we use such a code to calculate the wakefield of a sufficiently short bunch this wakefield can also be used as a Green's function. For example, if the longitudinal wakefield of the short bunch is $\mathcal{W}_{1z}$, then we can approximate the wakefield of a significantly longer bunch by

$$\mathcal{W}_z(s) = \frac{1}{Q} \int_{-\infty}^{\infty} ds'\ \rho(s-s')\ \mathcal{W}_{1z}(s') \quad . \tag{2.13}$$

It is interesting to note that if the two bunches are gaussian, with bunch lengths of σ_{1z} and σ_z respectively, and if $\sigma_z > \sigma_{1z}$, then $\mathcal{W}_z$ is given by

$$\mathcal{W}_z(s) = \frac{1}{\sqrt{2\pi}\sigma_{tz}} \int_{-\infty}^{\infty} ds'\ \mathcal{W}_{1z}(s') \exp\left(-\frac{(s-s')^2}{2\sigma_{tz}^2}\right) \quad , \tag{2.14}$$

where $\sigma_{tz}^2 = \sigma_z^2 - \sigma_{1z}^2$. Eq. (2.14) follows from a property of the convolution of

gaussians. Thus the longitudinal bunch wake of a gaussian can be used as a Green's function for any longer gaussian bunch.

There are other sources of wakefields in a linac, such as bellows, scrapers, position monitors. The wall resistance also contributes to a wakefield even in a smooth tube. But a linac is normally composed mostly of accelerating structure, and the effect of all these additional sources is normally small in comparison.

Much work has been published on wakefields over the years. This section was not intended to give a thorough treatment of the subject. Refs. 3, 10 and 11 are review articles on the subject. For relations that can be useful for scaling the wakefields of a bunch, see Ref. 2.

2.3 The Wakefields for the SLAC Structure

The SLAC accelerating structure is a cylindrically symmetric, disk-loaded structure, with wave length $\lambda_{RF} = 10.5$ cm, period $p = \lambda_{RF}/3 = 3.5$ cm and iris thickness of 0.6 cm. It is a constant gradient structure; the iris radius and cavity outer radius of every cell in a three meter section are unique. For calculating the wakefields this structure was modelled by the four parameter periodic structure shown in Fig. 1b. The dimensions used are those of the average SLAC cell; *i.e.* iris radius $a = 1.16$ cm and outer cell radius $b = 4.13$ cm.

The longitudinal wake was calculated by summing over modes according to Eq.(2.6).[4] The frequencies ω_{0n} and the loss parameters k_{0n} of 416 longitudinal modes were computed using the computer code KN7C.[12] But to be used as a Green's function for a bunch as short as 1 mm many more modes would need to be computed. However, for higher frequencies it is sufficient to know the statistical properties of the modes, which for a periodic disk-loaded structure can be represented by the so-called optical resonator model.[12–14] Based on this model an analytic extension was added to the modal sum to obtain the total wake.

The modal sum is given by the dashed curve in Fig. 2 (top), whereas the sum plus analytic extension is given by the solid curve. Note that the optical resonator model yields a wake W_z that is finite at the origin, in this case with a value of 8 V/pC/cell. The bottom frame of Fig. 2 shows the longitudinal wake on a longer time scale. Note that test particles at between 20 and 75 mm behind the exciting charge will gain rather than lose energy. The jaggedness in the wake after 38 mm indicates the beating of a few dominant modes. The dotdash curve gives the contribution of the fundamental mode only. We see that the long range behavior of the longitudinal wake is roughly given by the fundamental mode.

Similarly, the dipole wake potential was calculated for the SLAC structure according to Eq. (2.7) using modes computed by the program TRANSVRS.[15]

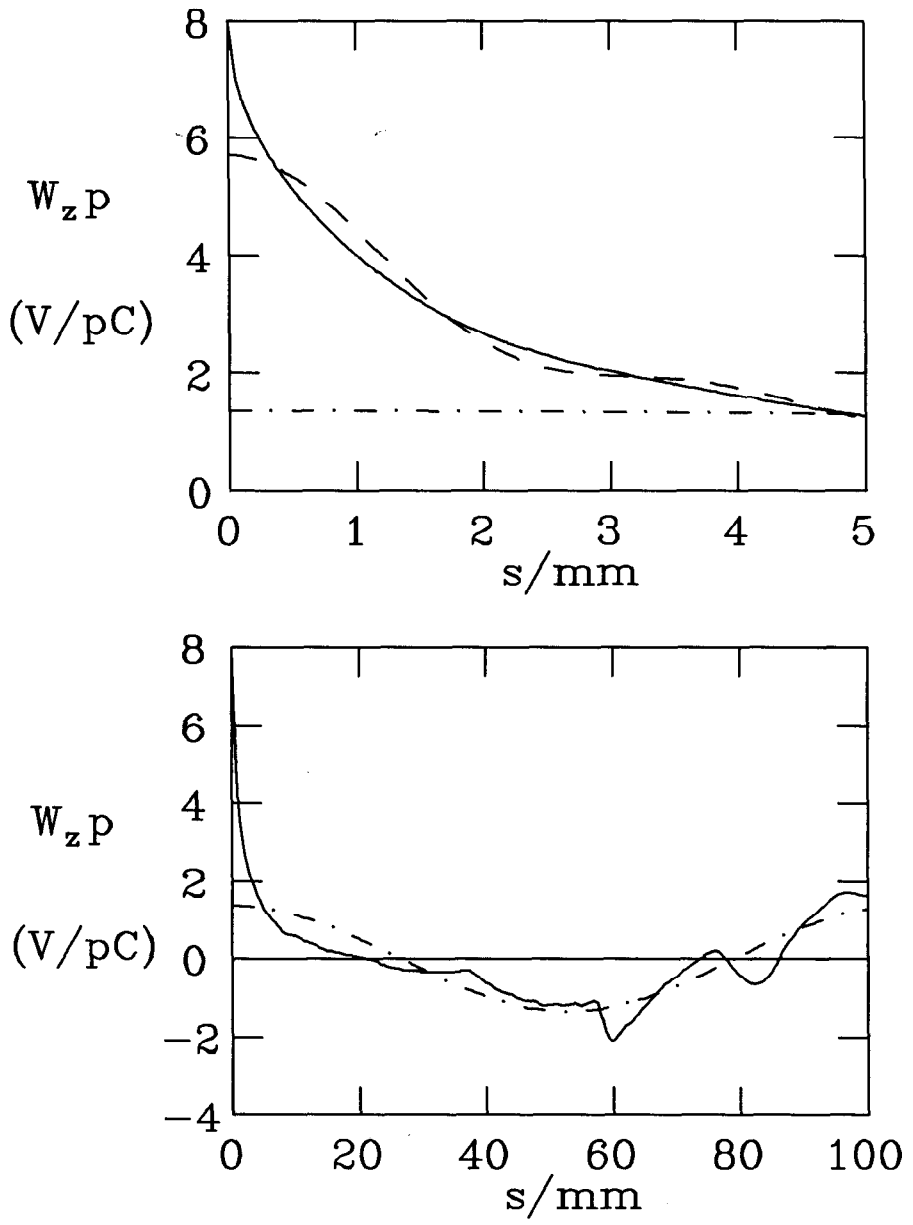

Fig. 2. Longitudinal delta-function wake per cell for the average SLAC cell for 0-5 mm (top) and 0-100 mm (bottom). The dashed curve in the top frame gives the sum of 416 modes only, whereas the solid curve includes the analytical extension. The contribution of the fundamental mode is given by the dotdash curve.

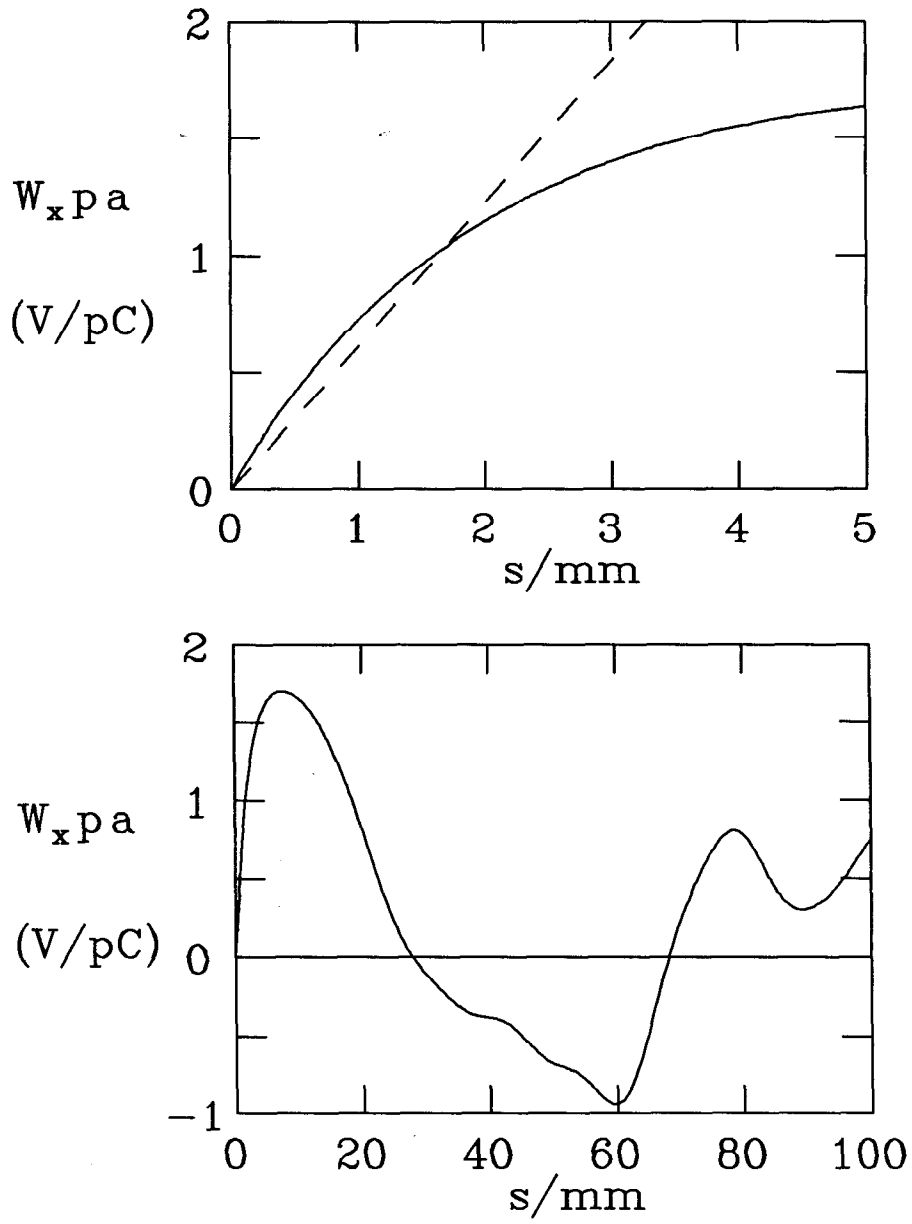

Fig. 3. Dipole wake per cell for the SLAC structure for 0-5 mm (top) and 0-100 mm (bottom). The dashed curve in the top frame gives a linear approximation to the wake seen by a 1 mm bunch.

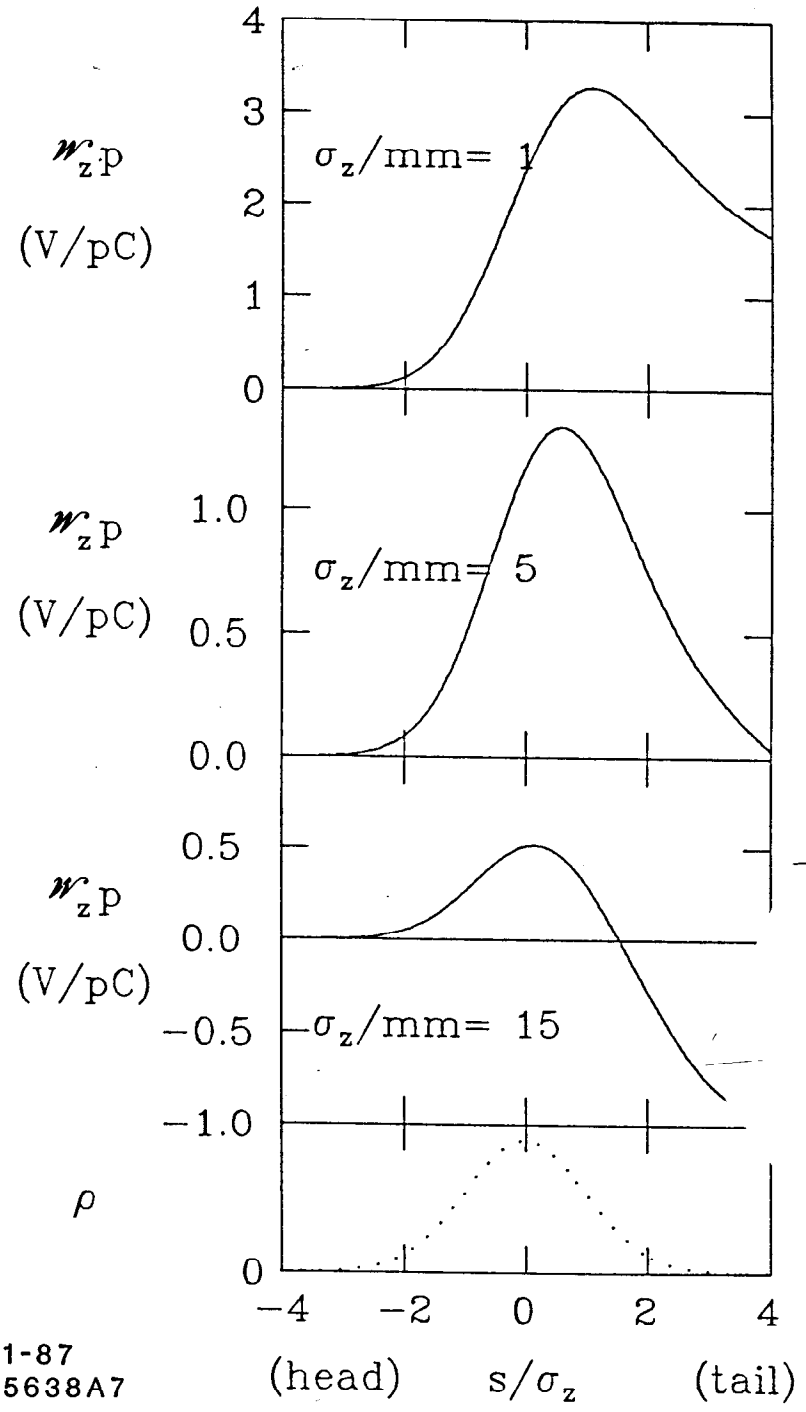

Fig. 4. The bunch wake per cell for gaussian bunches with σ_z of 1, 5, 15 mm (from top to bottom) in the SLAC structure. The dotted curve gives the charge distribution of the bunch. The head is to the left.

The sum for 56 modes plus analytic extension is shown in Fig. 3. In the top frame a linear approximation to the wake that is seen by a 1 mm bunch is shown (dashed). This linear approximation, after scaling to a higher frequency, will be used in the simulations of Chapter 4. The bottom frame shows the dipole wake on a longer scale. Again the ringing of a few of the lowest frequency modes can be seen beginning near 38 mm.

We see a general property of wakefields of cavities. The wakes can generally be divided into two parts: (i) The short range wake, which is smooth, takes many modes to approximate well. A time domain calculation, for example by using the time domain code TBCI with a very short bunch, is more natural over this range. It is the effects of the short range wake that concerns us in this paper. (ii) The long range wake tends to be choppy, and is well characterized by the ringing of a few dominant modes. A modal calculation is more natural over this range.

The convolution in Eq. (2.10) was performed yielding the bunch wakes for gaussian bunches with σ_z of 1, 5, 15 mm (see Fig. 4). The charge distribution of the bunch is given in the bottom frame. The head of the bunch is to the left. For short bunches (our main concern in this paper) all the particles of the bunch lose energy, as can be seen in the top frame. Across $\pm 1\sigma_z$ of the bunch the induced voltage is rather linear. As the bunch length is increased, not only is peak of $\mathcal{W}_z$ reduced but the shape of the induced voltage changes significantly. When $\sigma_z = 15$ mm the tail particles regain some of the energy lost by the front of the bunch.

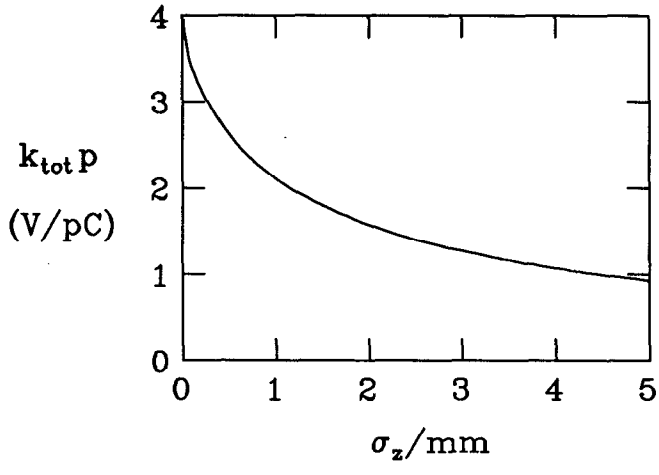

Fig. 5. The total loss parameter per cell as a function of bunch length for the SLAC structure.

The integration of Eq. (2.11) was performed, yielding k_{tot} for a gaussian bunch traversing the SLAC disk-loaded structure. The results are given as a

function of σ_z in Fig. 5. The energy loss decreases as the bunch becomes longer. Note that k_{tot} for zero bunch length equals $W_z(0)/2$.

3. LONGITUDINAL WAKEFIELD EFFECTS

An electron bunch loses energy when it traverses an accelerating structure due to wakefields. This loss is sometimes called beam loading. In the SLC (SLAC Linear Collider, see Ref. 16) the number of particles in a bunch is $N = 5 \times 10^{10}$, the bunch length is $\sigma_z = 1$ mm, the cell length is $p = 3.5$ cm and the total linac length is 3000 m. From Fig. 5 we see that for $\sigma_z = 1$ mm the total loss is 2.1 V/pC/cell. Therefore a total of 1.4 GeV is lost to the linac cavities. This reduces the effective accelerating gradient by 3% if the nominal final energy is 50 GeV.

Since the energy lost by a particle in the bunch depends on its longitudinal position, the wakefield induces an energy spread. Bunching and focusing effects of longitudinal modes are negligible for ultra-relativistic particles. In this paper we will not discuss multi-bunch effects. With a train of bunches the energy of the particles in a bunch is also affected by the wakefields of previous bunches.

3.1 Minimizing the Final Energy Spread

If a bunch sits on the crest of the RF wave it will receive an energy spread due to the curvature of the wave form, though for short bunches this effect is small. For a short, intense bunch, though, the longitudinal wakefield can introduce to a large variation in energy along the bunch. As can be seen by the example of a 1 mm bunch in the SLAC disk-loaded structure (see the top frame of Fig. 4) the induced wake is rather linear with the tail of the bunch losing more energy than the head. Since, however, the slope of the RF wave also looks quite linear to a short bunch, one can imagine that the energy spread can be compensated quite well by running in front of the crest, at least over a certain range of parameters.

Let the RF wave be given by $\hat{V}\cos(\omega_{RF}z/c)$. Then for short bunches the optimal phase to cancel the wakefield induced energy spread can be approximated by

$$\sin\phi_0 = -\frac{c}{\omega_{RF}\hat{V}}\int_{-\infty}^{\infty} dz\,\rho(z)W_z'(z) \quad , \tag{3.1}$$

where $W_z'(z)$ is the slope of the bunch wake and positive phase is ahead of the crest of the RF wave. The integral in the above expression is the average slope of the induced voltage. It depends linearly on the total charge Q and inversely on σ_z. Therefore as Q is increased and/or σ_z is decreased the right hand side of

Eq. (3.1) becomes larger. At some point ϕ_0 becomes so large that the beam is no longer getting a large portion of the available RF field, and this method of energy spread compensation loses its usefulness. Note that when the right hand side is greater than one Eq. (3.1) no longer has a solution.

We have used a computer code to find the optimal phase ϕ_0 that minimizes the energy spread in a gaussian bunch traversing the SLAC structure, taking $\hat{V} = 17$ MeV/m. The longitudinal wake of Fig. 2 was used in the calculation. The solutions for $N = 5 \times 10^{10}$ (solid) and $N = 7 \times 10^{10}$ (dashes) are given in the top frame of Fig. 6. The dotted curves give the approximate answer given by Eq. (3.1). The middle plot gives the resulting final energy spread when the initial energy is small compared to the final energy. In the bottom plot we see the ratio $V/\hat{V}$ of the net gradient to the gradient that would be experienced by a test particle sitting on top of the RF crest. This plot includes both the effects of beam loading and of the loss of energy due to running off the RF crest. We see that for $N = 5 \times 10^{10}$ and $\sigma_z = 1$ mm that $\phi_0 = 12°$, resulting in a final energy spread $(\sigma_E/E)_f$ of 0.4% and $V/\hat{V}$ of 0.95. By moving off the crest the energy spread has been reduced from 1.3% to 0.4%. Fig. 7 gives the energy variation along the bunch for this case. If the bunch length of 0.5 mm were chosen, then the bunch would need to run at $\phi_0 = 30°$ to reduce $(\sigma_E/E)_f$ to 0.6%. But then the effective accelerating gradient would only be 80% of the nominal value.

It should be pointed out that to minimize the energy spread it is only necessary that the bunch *on average* see the optimal slope of the RF wave. By inducing a larger coherent energy spread early in the linac but reducing it again later on, one can gain the beneficial effects of Landau Damping that will be discussed later.

Other work on compensating the induced energy spread by the slope of the RF wave is given in Refs. 16 and 17. In Ref. 18 the energy spread is made to be zero by properly shaping the bunch in addition to choosing the optimal RF phase. The cancellation of wakefield induced energy spread in longer bunches with W_z nearly symmetric about the bunch center is discussed in Ref. 19.

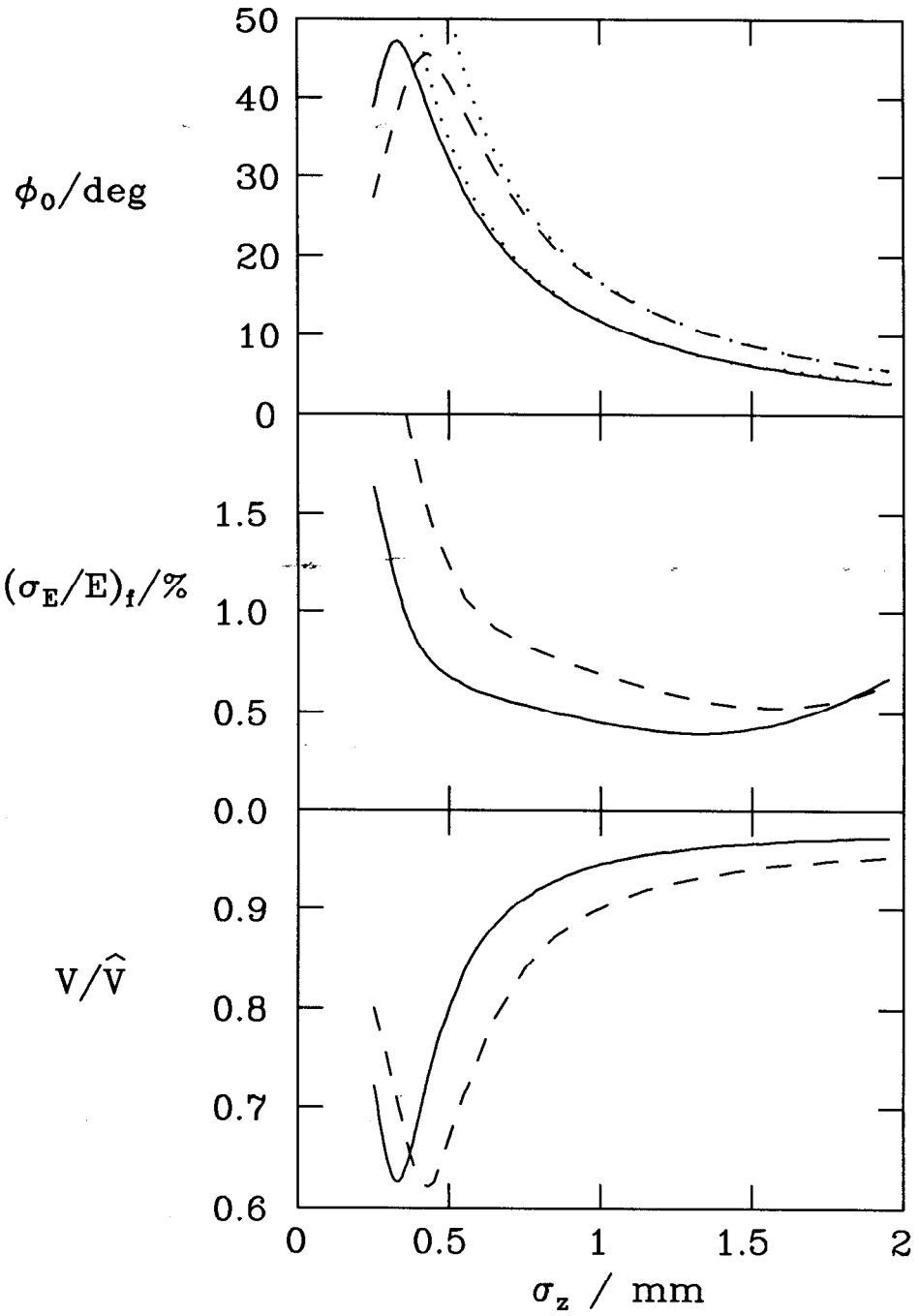

Fig. 6. The SLC: The optimal phase to minimize $(\sigma_E/E)_f$ (top), the resulting final energy spread (middle), and the ratio $V/\hat{V}$ (bottom) are shown *vs.* bunch length. $\hat{V} = 17$ MeV/m, and $N = 5 \times 10^{10}$ (solid) or 7×10^{10} (dashes). The approximate solution (Eq. (3.1)) is also plotted in the top frame (dots).

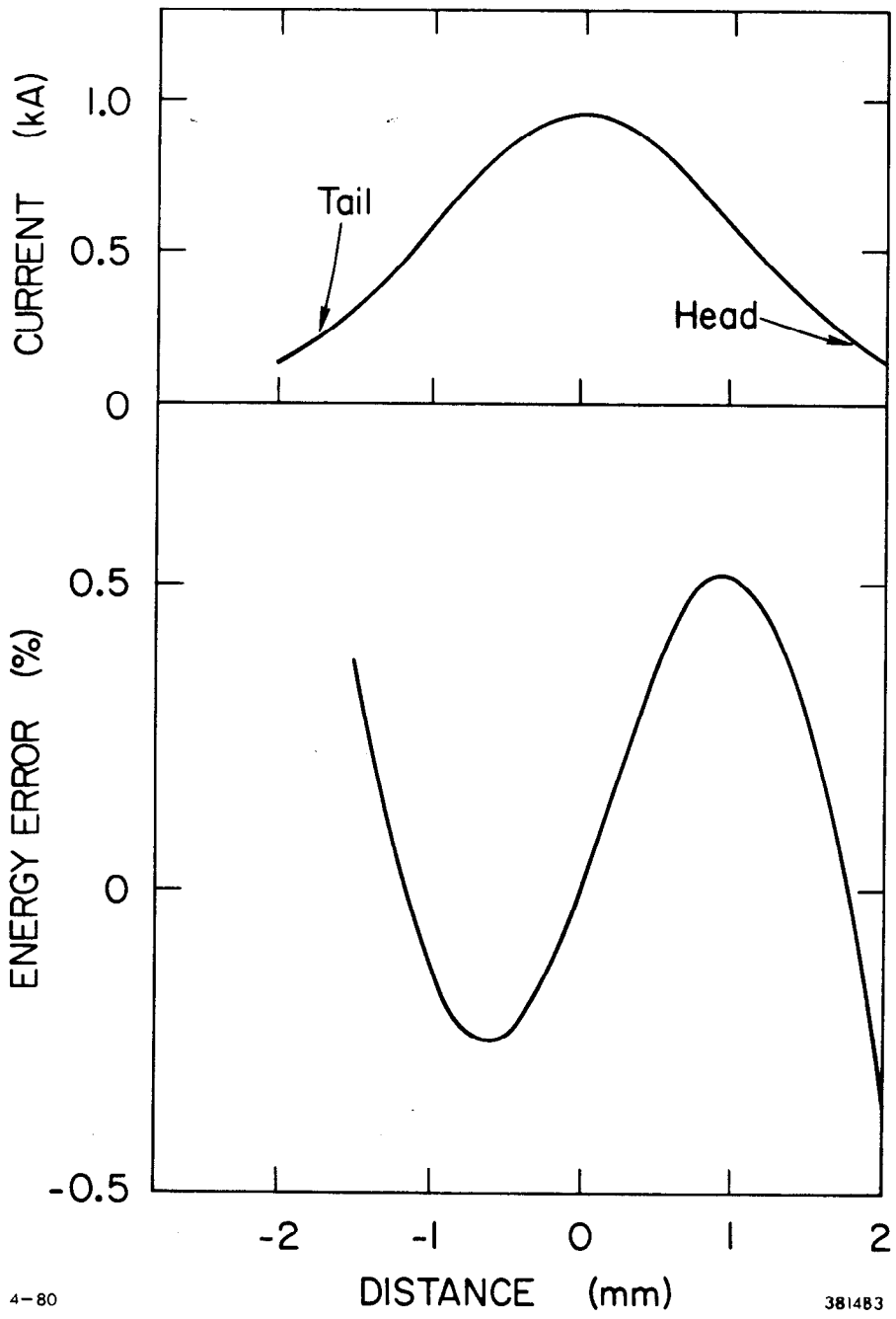

Fig. 7. The SLC: The final energy error along a gaussian bunch with $N = 5 \times 10^{10}$ and $\sigma_z = 1$ mm, and with the bunch at 12 ° in front of the RF crest. The charge distribution is given in the top frame.

4. TRANSVERSE WAKEFIELD EFFECTS

Consider an ultra-relativistic bunched beam traversing a collider linac with a cylindrically symmetric accelerating structure. We can think of the bunch as composed of many macro-slices, each with its center x, and with its transverse charge distribution about this center, characterized by its rms value σ_x. If the bunch does not stray too far from the structure axis, then a test slice is kicked by all preceding slices by an amount proportional to their charge, their offset from the axis and to the dipole wakefield of their longitudinal separation from the test slice. Since the dipole wake does not focus or defocus (it acts like a dipole magnet) the transverse size of the slices is not affected, assuming the slices are monoenergetic. Therefore we are justified in solving the equation of motion of the centers of the slices, without regard to their transverse charge distributions. After solving this problem we can add the transverse characteristics of the slices to the solution in order to discuss the emittance growth or the luminosity reduction.

Let us begin with the case of smooth focusing. The equation of motion for a test particle at longitudinal position z within the bunch, and at position s along the linac is

$$\frac{d}{ds}\left[\gamma(s,z)\frac{d}{ds}x(s,z)\right]+k^2(s,z)\gamma(s,z)x(s,z) = \frac{e}{mc^2}\int_z^\infty dz'\,\rho(z')W_x(z'-z)x(s,z') \quad , \tag{4.1}$$

with γ the energy, k the betatron wavelength, ρ the charge density and W_x the dipole wakefield. Note that the focusing strength is given by $k = 1/\beta = 2\pi/\lambda_\beta$ where β is the beta function and λ_β is the betatron wave length. (Note that s and z have different meanings here than in Chapter 2.)

Table 1 gives some parameters for a 300 GeV on 300 GeV collider with an acceleration gradient of 100 MeV/m (Case A). It is a somewhat modified version of the collider discussed by P. Wilson in Ref. 20. We will use this machine as our example for the simulations to be presented in this chapter. In this chapter we will approximate the wakefield by a linearly increasing function with slope W_x'. The accelerating structure is taken to be the SLAC linac structure, but scaled up a factor of four in frequency to 11.4 GHz. Therefore the transverse wakefield (when given in units of Volts/pC/m^2) increases by $4^3 = 64$. We further open the aperture sufficiently ($\sim 30\%$) to reduce the resulting wake by 60%. The simplified wake of the SLAC structure (the dashed curve in Fig. 3) has a value of 1.5 keV/pC/m^2 at a distance $\Delta z = \sigma_z = 1$ mm. Thus the wake at $\Delta z = \sigma_z = 0.25$ mm for the scaled collider is 39 keV/pC/m^2. For comparison the SLC parameters[16] are given in column B, although in the real machine λ_β is not kept constant. For simplicity the longitudinal wake will not be included in the simulations of this chapter.

Table 1. Parameters of two linear colliders

Parameter	A: 300 GeV Collider	B: Simplified SLC
initial energy, E_0	5 GeV	1.21 GeV
final energy, E_f	300 GeV	50 GeV
machine length, L	3000 m	3000 m
number of particles, N	1×10^{10}	5×10^{10}
betatron wave length, λ_β	50 m	100 m
RF wave length, λ_{RF}	2.6 cm	10.4 cm
bunch length, σ_z	0.25 mm	1.0 mm
dipole wake, $W_x'\sigma_z$	39 keV/pC/m^2	1.5 keV/pC/m^2

4.1 The Two-Particle Model

The two-particle model can be useful for studying single bunch beam break-up in a linac.[10,11] Let the beam be modelled by two macro-particles, each of charge $Q/2$ separated by a longitudinal distance $\Delta z = 2\sigma_z$. As a further simplification let us consider the case of no acceleration. The two particles have respectively wave numbers k, $k + \Delta k$, and energies E, $E + \Delta E$. (For smooth focusing $\Delta k/k = -\Delta E/E$.) Particle 1's equation of motion is simply

$$x_1'' + k^2 x_1 = 0 \quad , \tag{4.2}$$

where prime denotes differentiation with respect to s. It feels no transverse wake force and thus undergoes free betatron oscillation. Particle 2, though, experiences the force $F_x = eQW_x'\Delta z\, x_1/2$ due to the the off-axis motion of the leading particle. The equation of motion for particle 2 is that of a simple driven harmonic oscillator

$$x_2'' + (k + \Delta k)^2 x_2 = C x_1 \tag{4.3}$$

where $C = eQW_x'\Delta z/2E$ for $|\Delta E/E|$ small.

The effective emittance growth due to the dipole wakefield is modelled here by the displacement of the particles in phase space. Hence we would like to keep the quantities $|x_2 - x_1|$ and $|x_2' - x_1'|$ small. If both particles have the same initial conditions and $\Delta k = 0$ then

$$\frac{(x_2 - x_1)}{\hat{x}} = \frac{Cs}{2ik} e^{iks} \quad , \tag{4.4}$$

where $\hat{x}$ is a complex constant determined by the initial conditions. Eq. (4.4) is a linearly growing oscillation. The quantity $(x_2' - x_1')$ is just the derivative of Eq.

(4.4) and would therefore also be represented by a linearly growing oscillation, for large s. For small $|\Delta k/k|$ but with $\Delta k \neq 0$ we get

$$\frac{(x_2 - x_1)}{\hat{x}} = \left(1 - \frac{C}{2k\Delta k}\right) \; 2i \sin(\frac{\Delta k\, s}{2}) e^{i(k+\frac{\Delta k}{2})s} \; . \tag{4.5}$$

Eq. (4.5) represents two beating sine waves with amplitude $A = 2(1 - C/2k\Delta k)$. We see an asymmetry in the effect of the energy spread. For least growth, that is, to minimize A, we want $\Delta k > 0$: the trailing particle should have lower energy than the leading particle. In particular, if $A = 0$, that is if

$$\Delta E = -\frac{eQW_x'\Delta z}{4k^2} \; , \tag{4.6}$$

the trailing particle also undergoes pure betatron motion and exactly tracks the motion of the leading particle. In this case the extra phase advance of Particle 2 over a given distance, due to the difference in energy, exactly cancels the wakefield kick it feels due to Particle 1. Therefore there is no emittance growth.

We also note that both Eq. (4.5) and its derivative reach approximately zero for $\Delta k\, s/2 = n\pi$, where n is an integer. By a proper choice of Δk, one of these minima can be made to coincide with the end of the linac, thus minimizing the emittance there. Note that the point of zero crossing is independent of the sign of Δk.

From the two particle analysis we might expect that the energy spread necessary to effectively damp emittance growth in a bunch is

$$\sigma_E \approx \frac{eQW_x'\sigma_z}{4k^2} \quad , \tag{4.7}$$

with the head at higher energy than the tail. This is very similar to a relation given in Ref. 1 as an estimate of the energy spread needed for good damping in a linear collider. For our 300 GeV collider this relation yields $\sigma_E \approx 1$ GeV. Note that for a machine with constant quad strengths and constant quad spacings, k varies as $E^{-1/2}$. In such a case Eq. (4.7) indicates a constant value of σ_E/E would be optimal.

We can similarly construct a three-particle model which will yield a particular solution including the factor s^2 when the particles all have the same energy. In general an n-particle model will have as highest power of s a term with s^{n-1} when the particles all have the same energy. An n-particle model with energy spread yields quite complicated results.

We can also include acceleration in our two-particle model. Let us assume k is constant, the acceleration is constant, and the acceleration is adiabatic;

i.e. kE_0/g is large compared to one, with E_0 the initial energy of the beam and $g = dE/ds$ the accelerating gradient. For the 300 GeV collider we find $kE_0/g = 4$. The homogenous solution of Eq. (4.1) gives the motion of the lead particle:

$$\frac{x_1}{\hat{x}} = \sqrt{\frac{E_0}{E_f}}\, e^{iks} \quad , \tag{4.8}$$

with E_f the final beam energy. The factor under the radical in the above equation is called the adiabatic damping factor. In the absence of wakefields the betatron amplitude as well as the beam size decrease as $E^{-1/2}$ when k is kept constant. The particular solution of Eq. (4.1) becomes

$$\frac{(x_2 - x_1)}{\hat{x}} = \sqrt{\frac{E_0}{E_f}}\frac{C}{2ik}\left[\frac{E_0}{g}\ln\left(1 + \frac{gs}{E_0}\right)\right] e^{iks} \quad , \tag{4.9}$$

with the gradient $g = dE/ds$. Apart from the adiabatic damping the oscillation amplitude of the second particle only depends on s as a log function, whereas with no acceleration its dependence is linear. Note that the terms within the brackets approach s as the gradient approaches zero.

Another more general derivation of the threshold for effective Landau Damping in a bunch is given in Ref. 21.

4.2 A Perturbation Solution

In Ref. 22 a perturbation approach is used to solve Eq. (4.1) for a rectangular charge distribution under certain assumptions. The beam is assumed to be monoenergetic, the charge distribution is uniform over the length l (and zero elsewhere) with total charge Q and the wakefield grows linearly as $W_x(\Delta z) = W_x'\Delta z$. If the acceleration gradient is constant, and the betatron wave number k is also constant the solution is given by

$$\frac{x(s,z)}{x_0} = \sqrt{\frac{E_0}{E_f}}\, e^{iks} \sum_{n=0}^{\infty} \frac{1}{n!(2n)!}\left(\frac{\eta}{2i}\right)^n \quad , \tag{4.10}$$

as long as the acceleration is adiabatic. The strength factor η is given by

$$\eta = \left(\frac{1}{2} - \frac{z}{l}\right)^2 \frac{eQW_x'l}{kg}\ln\left[1 + \frac{gs}{E_0}\right] \quad . \tag{4.11}$$

The front of the bunch is at $z = l/2$. Note that η depends most strongly on z/l. This qualitatively agrees with beam break-up simulations where the tail of a bunch can be greatly perturbed whereas the front half of the bunch is only

slightly affected. Note also that η depends linearly on bunch length. It depends on s only as the log function. But when g becomes zero the strength factor depends on s linearly.

The sum is highly peaked at one term which depends on the value of η. We see that the $n = 0$ term represents free betatron oscillation, the $n = 1$ term gives the two-particle model, the $n = 2$ term gives a three particle model, and so forth. Therefore a single particle model is appropriate until $\eta \approx 4$, the two-particle model is then appropriate until $\eta \approx 48$, the three particle model until $\eta \approx 180$, etc. For η not small, Eq. (4.10) can be summed by asymptotic techniques giving[22]

$$\frac{x(s,z)}{x_0} = \sqrt{\frac{E_0}{6\pi E_f}}\eta^{-\frac{1}{6}} \exp\left(\frac{3\sqrt{3}}{4}\eta^{\frac{1}{3}}\right) \cos\left[ks - \frac{3}{4}\eta^{\frac{1}{3}} + \frac{\pi}{12}\right] \quad . \tag{4.12}$$

It is the exponential factor that characterizes single bunch beam break-up. Note that the phase also depends on the strength parameter η, with the tail lagging the head in phase.

In Fig. 8 the orbit of the $-\sigma_z$ point (at $\sigma_z = l/2\sqrt{3}$ behind the bunch center) as given by Eq. (4.12) is plotted for the 300 GeV collider of Table 1. The plot is normalized to the initial offset and the adiabatic damping factor has been taken out. With no wakefields the orbit is a pure cosine wave with amplitude one. With wakefields, we see that at the end of the linac the strength parameter $\eta = 45$ and that the normalized offset $x(-\sigma_z) = -9.0$. The three particle model, the $n = 2$ term in Eq. (4.10), yields -10.3.

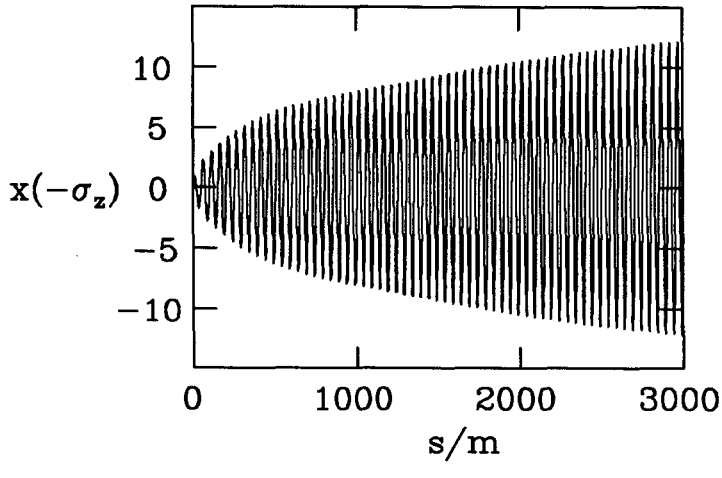

Fig. 8. The 300 GeV collider: The orbit of the $-\sigma_z$ point in a rectangular charge distribution as given by Eq. (4.12).

The perturbation method can be extended to find the orbit of a rectangular charge distribution with an energy spread.[23] The solution, though, is

quite complicated. A Laplace Transform method has also been used to solve the problem of this section, as well as the case when the wakefield includes a quadratic term.[24]

4.3 Smooth Focusing Simulation

If the longitudinal charge distribution of the bunch is gaussian, if the dipole wakefield is not a simple linear function, or if the bunch is not monoenergetic, the equation of motion (Eq. (4.1)) cannot be easily calculated by analytical methods. But the equation can be quite simply solved by a computer code.[25] First the bunch is represented by a finite number M of macro-particles. By writing the equation of motion in terms of x and $y = x'$ we are left with $2M$ coupled first order differential equations:

$$\begin{aligned} \frac{dy_i}{ds} &= -k^2 x_i - \frac{g_i y_i}{mc^2} + \frac{1}{E_i} \sum_{j<i}^{M} eQ_j x_j W_x(z_j - z_i) \\ \frac{dx_i}{ds} &= y_i \end{aligned} \quad , \tag{4.13}$$

with the gradient $g_i = dE_i/ds$. The bunch is taken to be moving in the positive z direction; the first slice is slice No. 1. Note that the sum is only over the slices ahead of the i^{th} one.

We have written a computer code to solve these equations using a Runga-Kutta method. For our simulations we represent the bunch by 41 macro-particles evenly spaced in z with a gaussian variation of intensity. The longitudinal wakes are not included. The gaussian is truncated at $\pm 2\sigma_z$. To simulate emittance growth due to injection jitter, the beam enters one unit off axis into a smooth focusing structure with no errors.

In Fig. 9 (top) we see the distribution of the macro-particles in phase space at the end of the 300 GeV linac, when there is no energy spread in the beam. A cross represents each macro-particle, with the head (at $z = 2\sigma_z$), center ($z = 0$) and tail ($z = -2\sigma_z$) macro-particle denoted respectively by the letters H, C, T. Both the abscissa and the ordinate are normalized by the adiabatic damping factor $(E_f/E_0)^{1/2}$. Without wakefields all particles would move together on the unit circle in the clockwise direction as they proceed along the linac; at the end (at $s = 60\lambda_\beta$) they would sit at position $x = 1$, $x' = 0$. With wakefields we see that much growth has occurred in the tail. The $-\sigma_z$ point (σ_z behind the bunch center) is at an amplitude of 10 times the free betatron oscillation amplitude. As we move from the head to the tail the particles lag more and more in phase. Note that in this plot the head and tail are on opposite sides of the x axis. The center frame shows the beam in the $z - x$ plane. In the bottom plot we see the

orbit of the $-\sigma_z$ macro-particle as it moves along the linac. Again the adiabatic damping factor has been removed. This plot looks very similar to Fig. 8, the results for a rectangular distribution as given by Eq. (4.12). At the end of the linac $x(-\sigma_z) = -10.3$.

Next the beam was injected into the linac with a linearly varying energy spread, with the head at a higher energy than the tail. Thus the energy of slice i is given by

$$E_i = E + z_i \frac{\sigma_E}{\sigma_z} \quad , \tag{4.14}$$

with E the energy of the central slice. This sign of energy spread will tend to cause the tail to advance in phase with respect to the head, thus compensating for the phase lag due to the wakefields.

The development of phase space as the beam moves down the 300 GeV linac with $\sigma_E = 0.75$ GeV is shown in Fig. 10. The wave number of the central slice is denoted by k_0. The beam begins by forming a loop near its center. Note that the sense of the phase variation, as one moves from the head to the tail, has changed: rather than in the counter-clockwise direction (lagging in phase) one now moves clockwise (advancing in phase). As the beam progresses, the amplitude of the tail decreases, and the beam wraps itself more and more around in phase space. From these phase space plots one can imagine that a two- or three-particle model is far less useful for a beam with energy spread than for one without. At $s = 60\lambda_\beta$ the head and tail are near the free betatron amplitude, whereas the core of the beam (that part from $-\sigma_z$ to σ_z) is at amplitudes significantly less than this value. Rather than just inhibiting emittance growth, the effect of the energy spread actually damps the core of the beam toward the structure axis.

The top frame of Fig. 11 shows the beam in the $z - x$ plane at the end of the linac. One clearly sees the damping of the beam core. In the bottom frame we see the orbit of the $-\sigma_z$ macro-particle. Note that the oscillation at first grows and then reduces to a value less than 0.5.

Fig. 12 gives the phase space at the end of the linac for different amounts of energy spread, with again the head at higher energy than the tail. At $\sigma_E = 0.25$ GeV the tail has not been reduced significantly. A small loop has formed near the bunch head. At $\sigma_E = 0.5$ GeV the core of the beam is all within the aperture of the free betatron amplitude at the end of the linac.

Fig. 13 (top) gives the phase space at the end of the machine when $\sigma_E = 0.75$ GeV, but with the sign of the energy variation reversed; *i.e.* the tail is given more energy than the head. In this case the tail spirals around the head in the natural (counter-clockwise) direction. It can be seen that beam break-up is not nearly as effectively inhibited as when the head has more energy than the tail. In the middle frame we see a snapshot of the beam in the $z - x$ plane. The

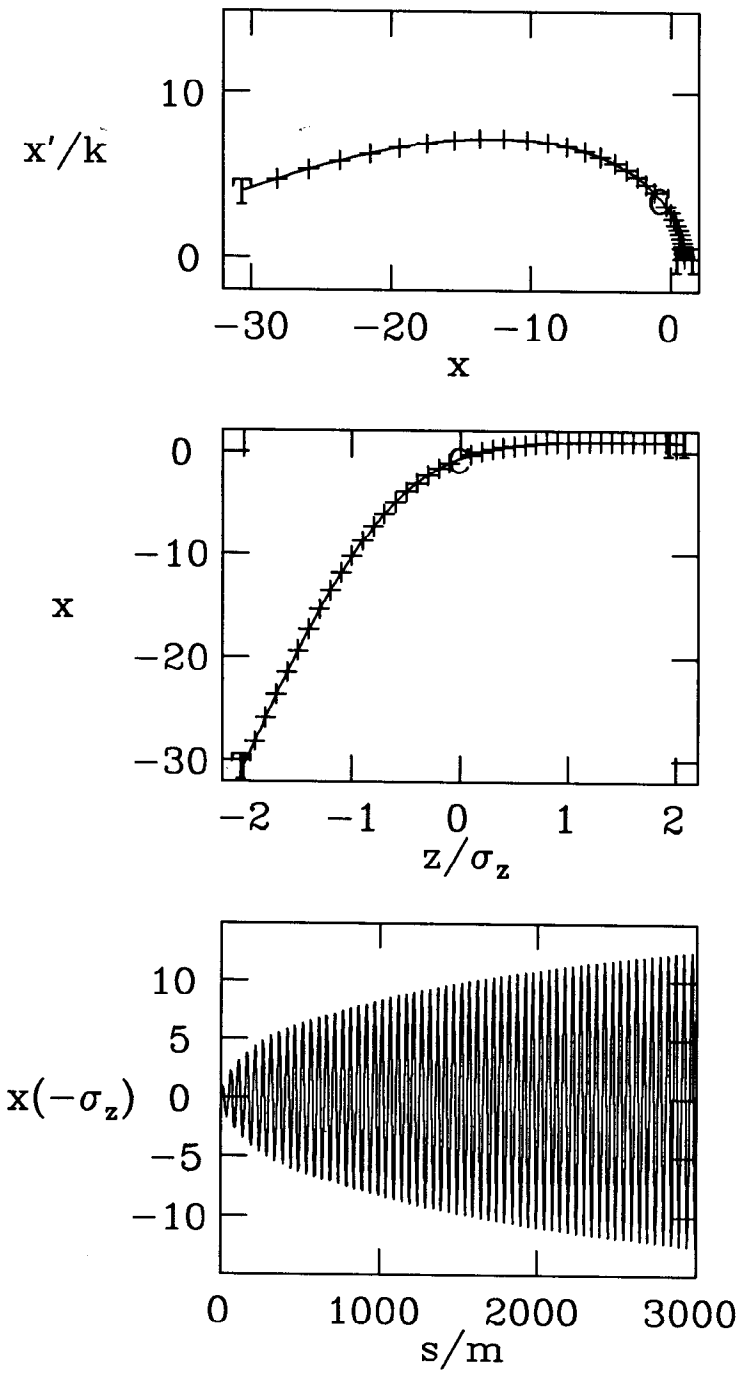

Fig. 9. Case A: Results for the case with no energy spread; the beam in phase space (top) and in the $z - x$ plane (middle) at the end of the linac, and the orbit of the $-\sigma_z$ slice (bottom).

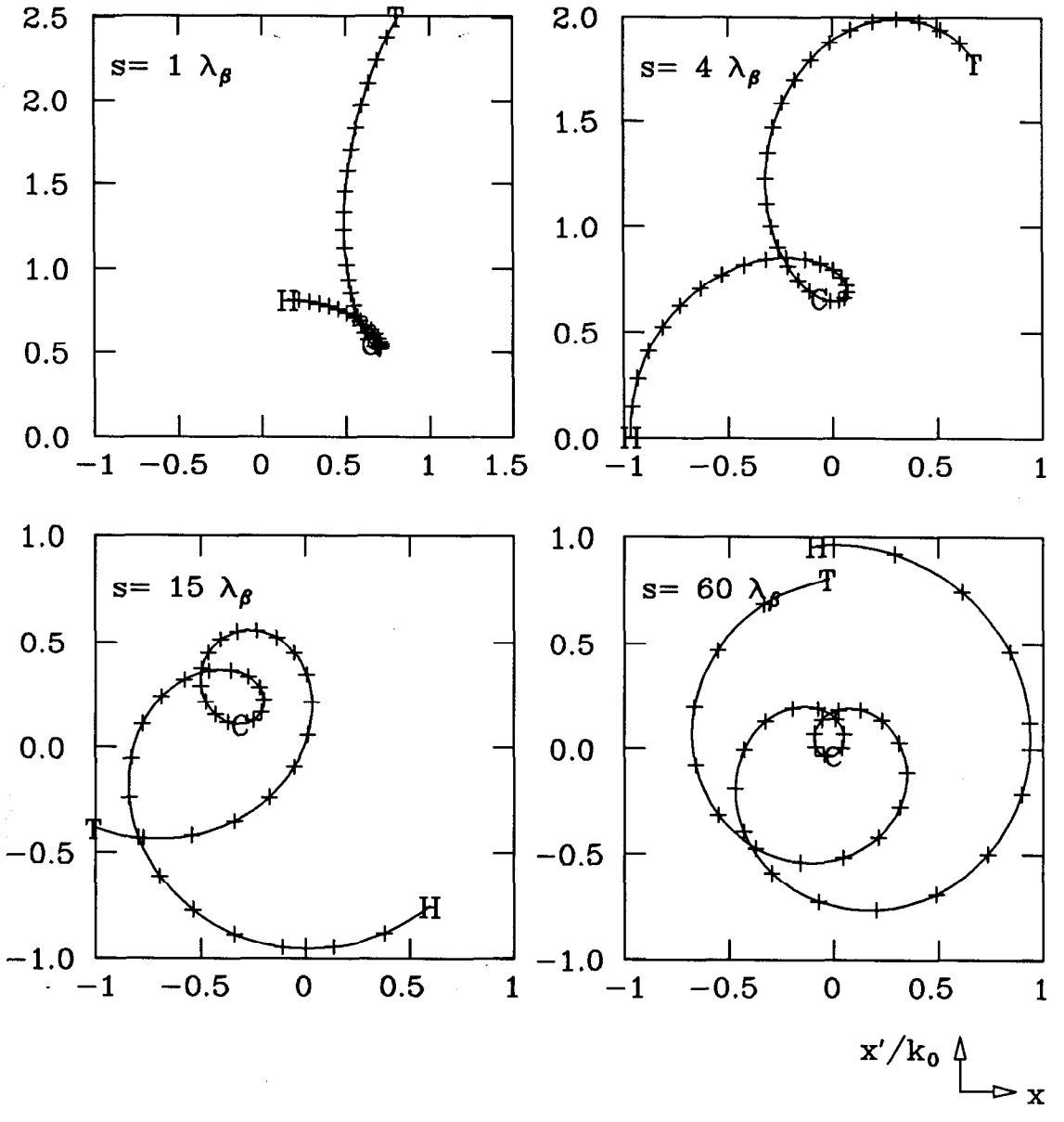

Fig. 10. Case A: The development of phase space along the linac for $\sigma_E = 0.75$ GeV, with the head at a higher energy than the tail.

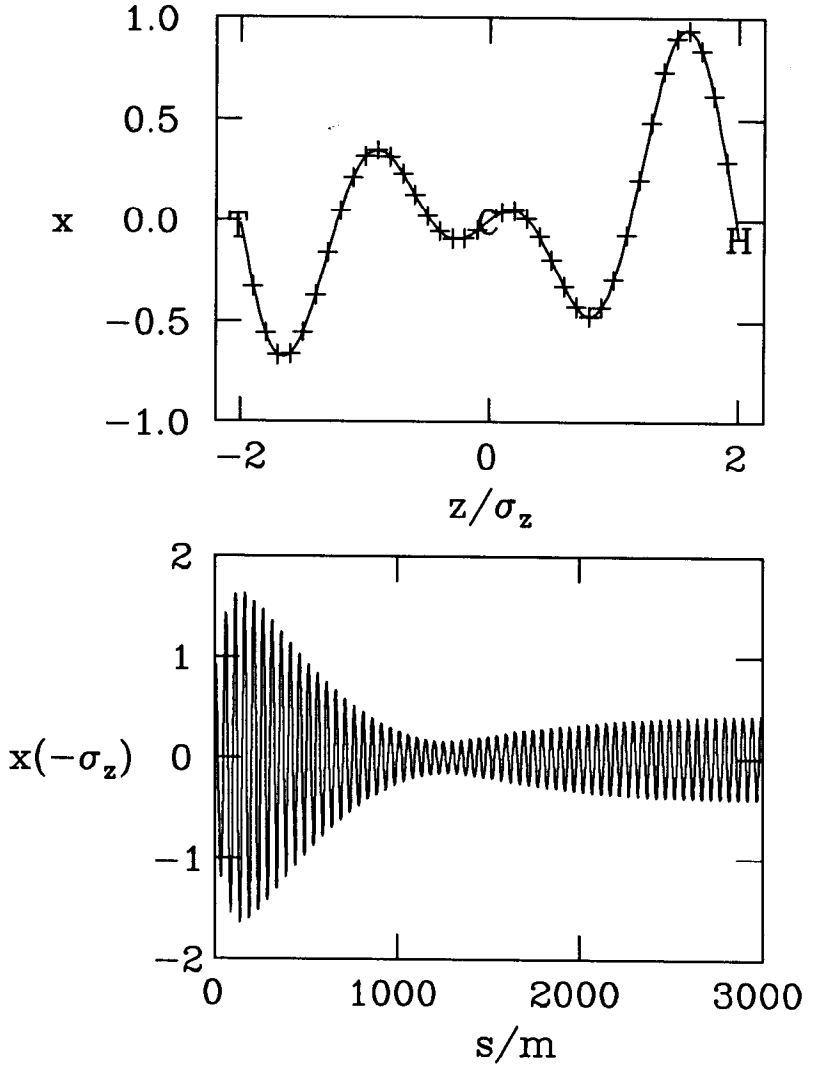

Fig. 11. Case A: The beam in the $z - x$ plane at the end of the linac (top) and the orbit of the $-\sigma_z$ slice (bottom) when $\sigma_E = 0.75$ GeV.

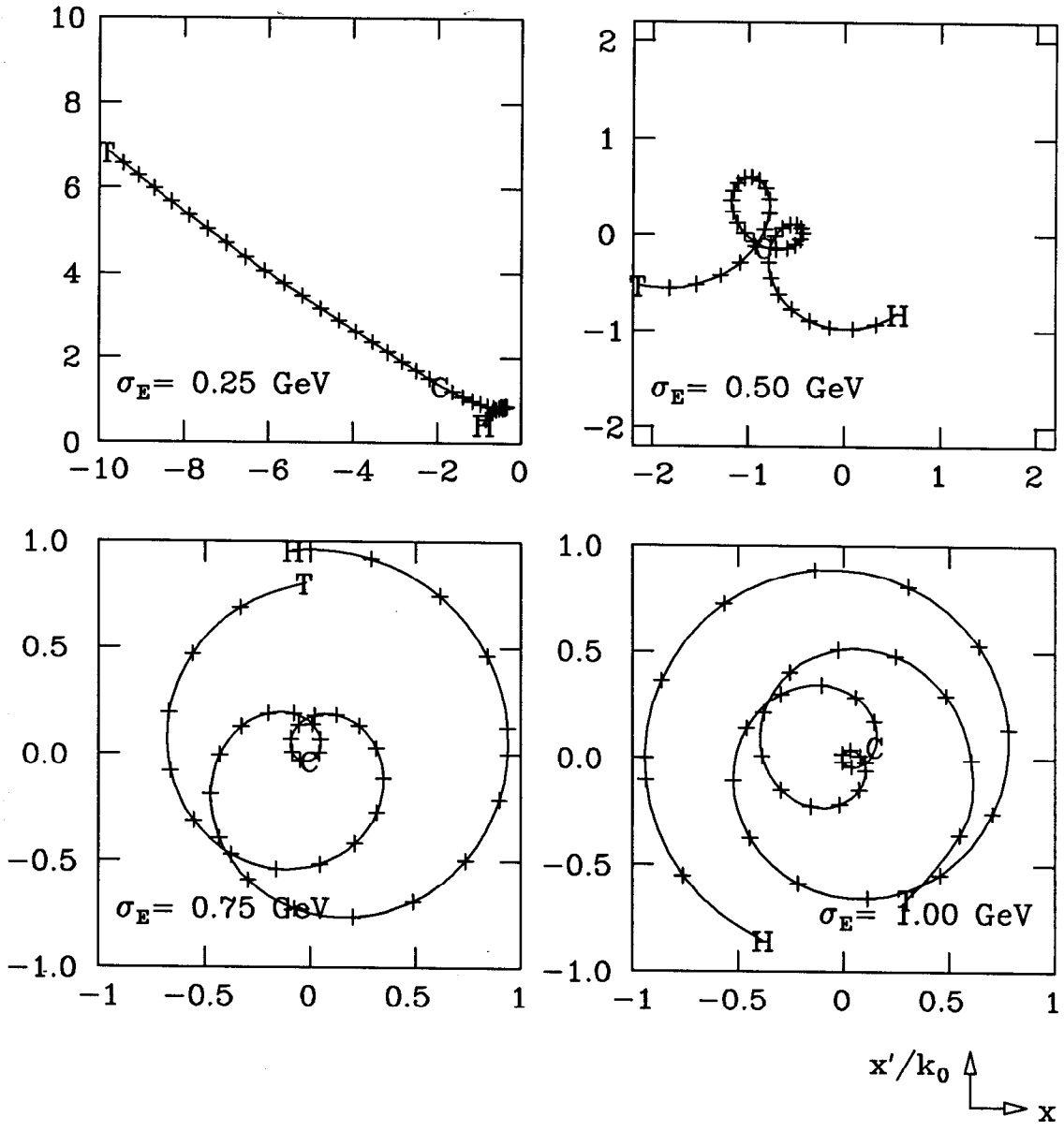

Fig. 12. Case A: Phase space at the end of the linac for beams with linearly varying energy spread. In all cases the head is at a higher energy than the tail.

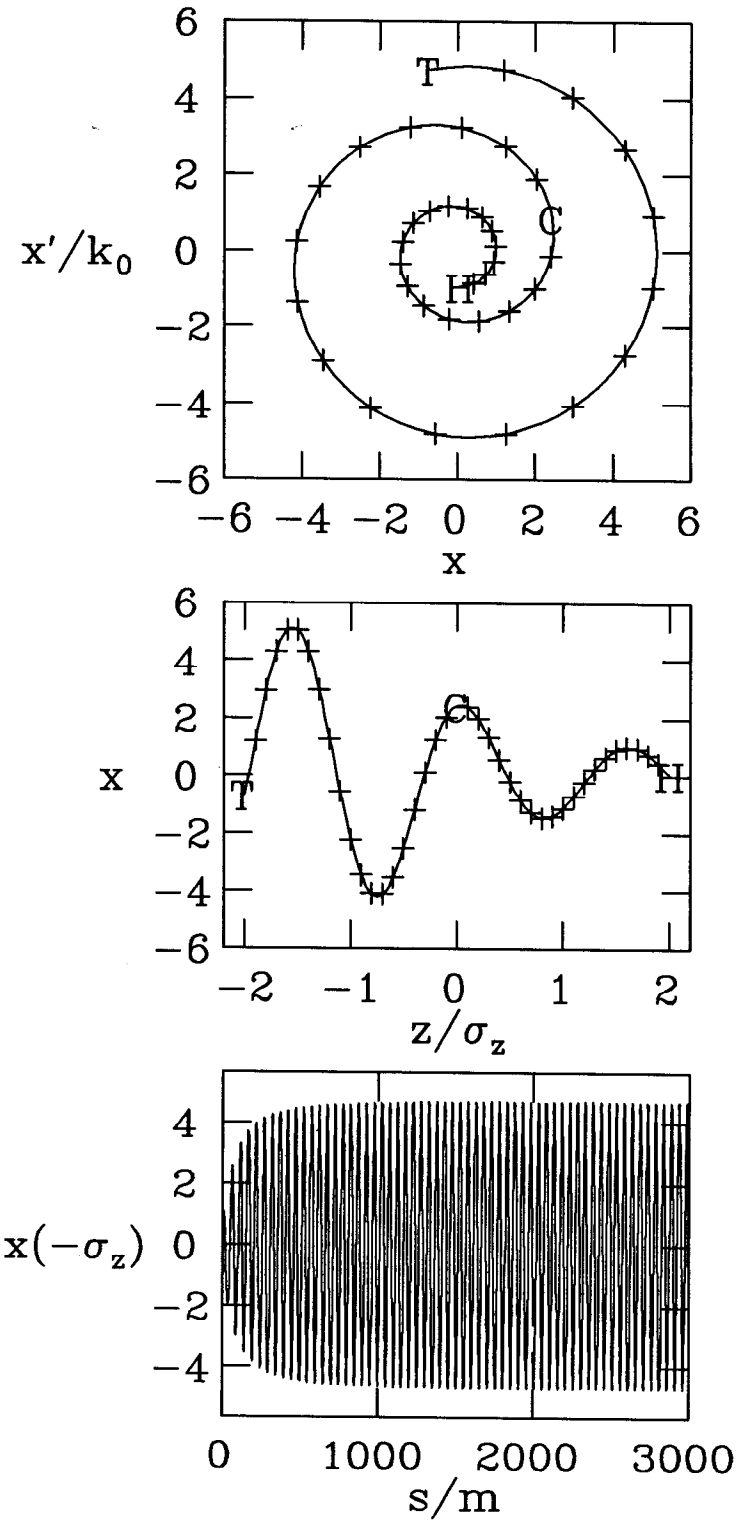

Fig. 13. Case A: Phase space (top) and $z - x$ plane (middle) at the end of the linac; orbit of the $-\sigma_z$ slice (bottom) with $\sigma_E = 0.75$ GeV, but with the head at lower energy than the tail.

oscillation amplitude grows as one moves to the tail of the bunch. The bottom frame gives the orbit of the $-\sigma_z$ slice. Its oscillation amplitude grows quickly to a constant value.

In addition to Ref. 25, Refs. 26 and 27 also have used smooth focusing simulation to study transverse beam dynamics including transverse wakefields for future linear colliders.

4.4 Measures of Beam Quality

Suppose the bunch enters the linac with an initial offset x_0. The simplest figure of merit for beam degradation is the x offset of a certain slice of the bunch at the end of the linac, divided by the transverse size σ_x of this slice. For the $-\sigma_z$ slice to be offset by less than σ_x at the end of the linac was taken as criterion for acceptable emittance growth in the SLC Design Report.[16] This figure of merit has the great advantage that it scales linearly with x_0. But it only gives a rough estimate of the emittance growth. In addition, one must search for the maximum value of this indicator near the end of the linac: it is possible that this indicator is nearly zero at the end of the linac while x' of the indicator slice is very large.

We can define an effective normalized emittance growth factor as

$$\varepsilon = \frac{\gamma}{\gamma_0 x_0^2 Q} \sum_i^M Q_i \left(x_i^2 + (x_i'/k_0)^2\right) \quad , \tag{4.15}$$

with γ the energy of the central slice and γ_0 the initial beam energy. Every slice contributes to the effective emittance in proportion to its charge and the area its position in phase space traces when rotated about the origin. Our emittance is independent of x_0; it is normalized in such a way that when there are no wakefields it will remain essentially at a value of one. One normally wants to compare the phase space area of the perturbed beam with that of an unperturbed beam. This can be simply done by multiplying ε by $(x_0/\sigma_{x0})^2$, with σ_{x0} the initial beam size.

Note that this definition of emittance growth is not very useful for studying the effect of a static injection error on luminosity. For example, if there is no wakefield and no energy spread a static injection error causes no emittance growth and can be perfectly corrected at the end of the linac by steering. Our emittance growth factor ε, however, yields a value of one; and it does not differentiate this case from the case with no wakefields and with energy spread, if σ_E/E is small. The latter case, however, is not so easily correctable if the total phase advance of the head differs significantly from that of the tail. Precisely which definition of effective emittance is most useful depends on the particular

application. The definition given here is simple and can be useful for studying jitter. The product $\varepsilon(x_0/\sigma_{x0})^2$ gives a measure of the average luminosity reduction over many pulses, for an injection jitter of amplitude x_0. A result of $\varepsilon < 1$ means the average luminosity reduction over many pulses is less than in the case with no wakefields.

In Fig. 14 we see the development of the emittance as the beam progresses down the 300 GeV linac for four values of energy spread, with the head at higher energy than the tail. When there is no energy spread ε continues to grow along the whole machine. When there is sufficient energy spread, however, the emittance first grows and then decreases. At $\sigma_E = 0.75$ GeV the emittance first grows to 1.4 at the beginning of the linac but then settles down to the value of 0.2.

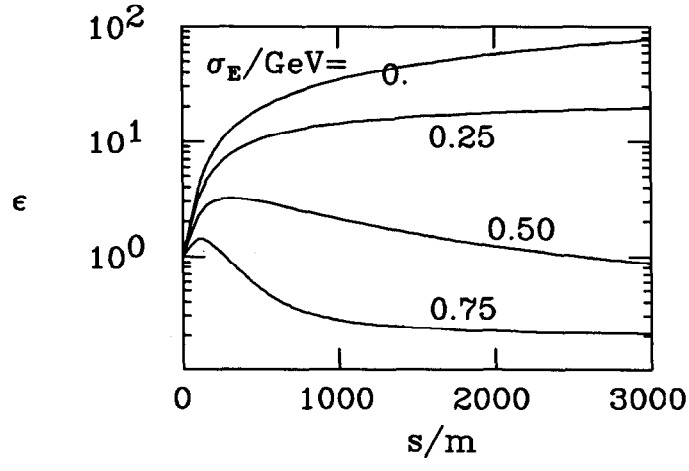

Fig. 14. Case A: The effective emittance as a function of s for several values of σ_E, with the head at a higher energy than the tail.

Fig. 15 gives the effective emittance growth as a function of energy spread at the end of our example linac with smooth focusing. The solid curve represents the case when the head is at a higher energy than the tail. The curve drops sharply as a function of σ_E. Note that the effective emittance is greater with no wakefields than it is with wakefields when $\sigma_E \gtrsim 0.5$ GeV. The two-particle criterion, Eq.(4.7), yields $\sigma_E \approx 1$ GeV, overestimating the threshold for optimal damping by about a factor of two. The dashed curve shows the emittance growth when the energy spread is of the opposite sign. (Note that an emittance curve similar in character to this one is given for the VLEPP linear collider in Ref. 1.)

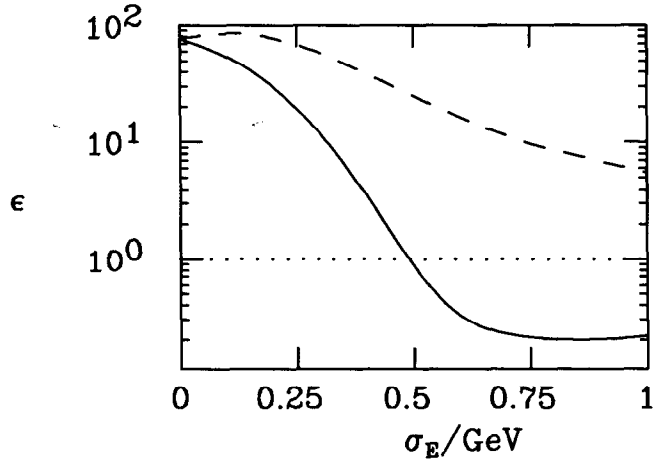

Fig. 15. Case A: Final ϵ as a function of σ_E with the head at higher (solid) or lower (dashes) energy than the tail. The dots give the no wake case.

One problem with taking ϵ as indicator of luminosity reduction is that it overestimates the effect of large excursions of the tail particles. To overcome this problem we can define a luminosity reduction factor as

$$r = \frac{\sigma_x^2}{Q} \sum_i^M \frac{Q_i}{x_i^2 + (x_i'/k_0)^2 + \sigma_x^2} \quad , \tag{4.16}$$

with σ_x the beam size of the central slice. Like an emittance, r is a smoothly varying function of s. Unlike ϵ, the luminosity reduction factor is a function of the beam size, which serves as a cut-off in the sum, so that r is never greater than one. Note that for growth that is small compared to σ_x we have

$$r \approx 1 - \varepsilon \left(\frac{x_0}{\sigma_{x0}} \right)^2 \quad . \tag{4.17}$$

In Fig. 16 we plot r as a function of x_0/σ_{x0} for energy spreads of 0., 0.50 and 0.75 GeV. The dotted curve gives the results with no wakefields. With a jitter amplitude $x_0/\sigma_{x0} = 1$ the luminosity factor r is reduced to 0.86 if $\sigma_E = 0.75$ GeV. With the same initial conditions $r = 0.16$ if there is no energy spread (which, however, is not so pessimistic as $1/\epsilon = 0.01$ as given by Fig. 15). With no wakefield r is 0.50 with the same initial condition.

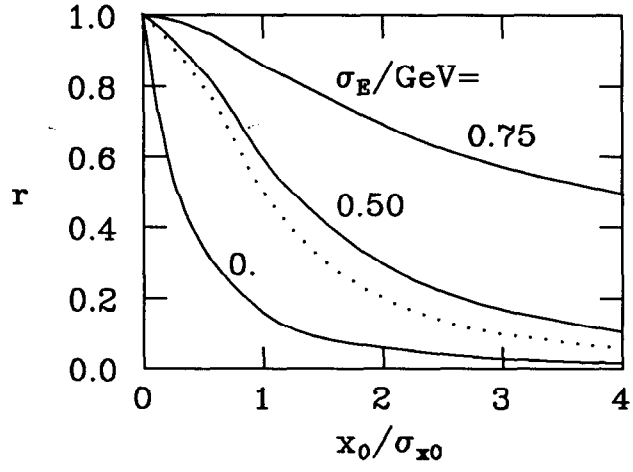

Fig. 16. Case A: The luminosity reduction factor r at the end of the linac for several values of σ_E, with the head at a higher energy than the tail. The dotted curve gives r in the absence of wakefields.

4.5 Simulation with Discrete Focusing Elements

Typically, a collider linac will be composed of mostly acceleration structure with an evenly spaced array of quadrupoles thrown in for focusing. Since the focusing is not continuous along the accelerator one would expect beam break-up to be worse in such a machine than in an idealized smooth focusing machine with the same value of betatron wave length. A method of tracking the single bunch behavior in a linac, including wakefields is described in Ref. 28. The computer code LTRACK, which employs this method, divides a bunch of charged particles into a number of slices longitudinally. It transports each slice's centroid vector (x, x', y, y') and sigma matrix (a 4×4 matrix describing the 4 dimensional transverse beam shape) through a lattice to first order by matrix multiplication. (See for example Ref. 29.) The program also keeps track of the energy of the slices (each slice is assumed to be monoenergetic). It assumes that the slices do not move longitudinally with respect to each other, a good approximation for high energy linacs. Unlike in the smooth focusing program, the effects of beam mismatch to the machine, and the effects of errors in the placements and strengths of the various lattice elements can be easily studied.

When traversing an acceleration section the centroids in either plane of a bunch normally transform as

$$\begin{pmatrix} x \\ x' \end{pmatrix}_1 = \begin{pmatrix} 1 & \frac{\ell}{\delta}\ln(1+\delta) \\ 0 & \frac{1}{1+\delta} \end{pmatrix} \begin{pmatrix} x \\ x' \end{pmatrix}_0 \quad . \tag{4.18}$$

The parameter ℓ in the matrix (called the transfer matrix) is the length of the section and $\delta = \Delta E/E$, with ΔE the unloaded energy gain in the section. It is

assumed that δ is small compared to 1. When the longitudinal wake is included the change in energy of the i^{th} slice becomes

$$\begin{aligned}\Delta E_i =& \Delta E - \frac{1}{2} e\ell Q_i W_z(0) - \sum_{j<i}^{M} e\ell Q_j W_z(z_j - z_i) \\ =& \Delta E - e\ell Q \mathcal{W}_z(z_i)\end{aligned} \quad , \tag{4.19}$$

with $W_z(z)$ is the longitudinal wake and $\mathcal{W}_z(z)$ the bunch wake at position z. The second term on the right of the top line of Eq. (4.19) represents the energy loss of slice i itself. For each slice the results of Eq. (4.19) are used to calculate $\delta_i = \Delta E_i / E_i$ which in turn is used to calculate the transfer matrix. The dipole wakefield affects the angle of slice i as

$$\Delta x_i' = \frac{1}{E_i} \sum_{j<i}^{M} e\ell Q_j x_j W_x(z_j - z_i) \quad , \tag{4.20}$$

where x_i is the transverse offset of slice i and $W_x(z)$ is the dipole wake at position z. Since this is a thin lens approximation longer acceleration sections may need to be cut into smaller pieces, with the longitudinal and dipole effects applied alternatively. It can be seen that LTRACK needs the longitudinal and dipole wakefields of the acceleration structure as input.

We have used LTRACK to calculated the effective emittance growth as a function of energy spread for the 300 GeV collider of Table 1. The lattice is a FODO type with thin lens quadrupoles and a phase advance of 90° per cell. To compare with the smooth focusing results the other conditions are the same as in the previous section. Again 41 slices over the interval $[-2\sigma_z, 2\sigma_z]$ represent the bunch. The longitudinal wakefield is not included: the beam enters the linac with an (absolute) energy spread that does not change as it progresses down the machine. The dipole wake is again given by its linear approximation. The results can be seen in Fig. 17. The dotted curve gives the smooth focusing results for comparison. Note that although with no energy spread ε is a factor of two larger in the discrete than in the smooth focusing case, the difference disappears by $\sigma_E = 0.5$ GeV. The difference at low values of σ_E is mostly due to growth in the bunch tail. With no energy spread, and at $x_0/\sigma_{x0} = 1$ the smooth focusing case yields $r = 0.16$ at the end of the linac whereas the discrete case gives $r = 0.14$.

As discussed before, the beam also loses energy to the dipole wakefields. But for beams that stay near the structure axis this energy loss is very small compared to that of the monopole wake and can usually be ignored. If desired, however, this effect can easily be included in the calculation. The higher moments of the transverse beam distribution will also drive higher moment

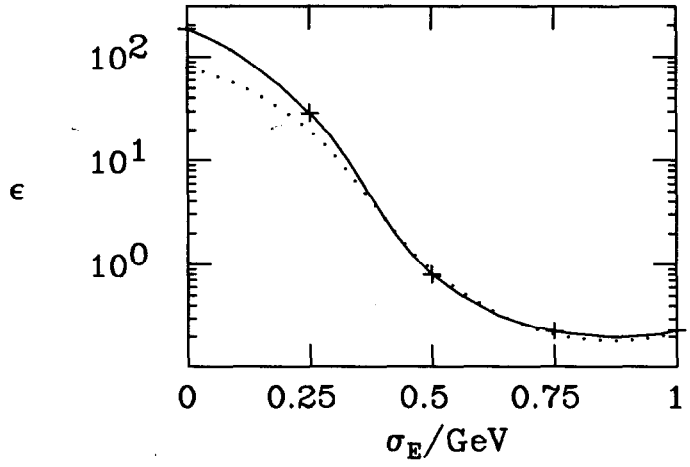

Fig. 17. Case A: Emittance growth for a FODO lattice with 90° per cell. The computed values are given by crosses. The dotted curve gives the smooth focusing results.

wakefields, but again these are small when the beam remains close to the axis. The quadrupole wake which, in addition to affecting their centroids, also tends to distort the profiles of the slices, can also be incorporated into the matrix formalism discussed in this section.[28]

4.6 FURTHER DISCUSSION

We have shown some wakefield effects and the effects of Landau Damping in a linear collider. The work on the simple 300 GeV collider presented here can be extended in several ways. For example, we can vary the betatron wave length near the beginning of the linac. If we reduce λ_β at the beginning of the linac we will reduce the initial energy spread σ_E/E needed for good damping from the value of 15% (0.75 GeV/5 GeV) given in our example. According to Eq. (4.7) the optimal energy spread should reduce by a factor of 4 when reducing λ_β by a factor of 2. At some point the real wakefield of a structure, rather than the linear approximation, should be included in the simulation. The longitudinal wake needs to be included. And further, the effects of errors, including orbit correction, need to be considered.

5. A MORE DETAILED EXAMPLE: THE SLC[30]

In the SLC, after leaving its damping ring, the electron (or positron) bunch is accelerated from 1.2 GeV to 50 GeV in sectors 2-30 of the linac, before entering the collider arcs. It is important that the beam emittance growth in these sectors be small. For 5×10^{10} particles per bunch slight excursions from the structure axis will induce dipole wake forces that will tend to cause large emittance growth. Position monitors and correctors are installed that will help keep the beam close to the structure axis. Further, instrumentation will be added that will allow the initial x, x', y, y' of the beam to be varied, to compensate coherent effects of machine errors,[22] until the best quality beam reaches the end of the linac. These measures, however, will have no effect on the pulse-to-pulse jitter of injection, whose tolerances turn out to be quite stringent in the SLC. According to calculations,[16] the allowable jitter amounts to 1% of σ_{x0} positional and 1% of $\sigma_{x'0}$ angular injection errors, either of which results in an emittance growth of 25%.

In the SLC the beam leaves the damping ring with very little energy spread. We propose running the bunch behind the crest of the RF wave in the early part of the linac, in order to induce a large coherent energy spread between the head and the tail of the bunch. This energy spread induces a damping similar to Landau damping that stabilizes the beam against the large transverse wakefields. This extra energy spread is gradually removed by placing the bunch at a suitable position in front of the crest of the RF wave in the later part of the linac. We shall see that this phase juggling results in greatly relaxed injection jitter tolerances, but at the cost of some final energy.

5.1 THE EFFECTIVE EMITTANCE

For this study we define the total effective x-emittance of a bunch

$$\epsilon_x^2 = \sigma_{xx}\sigma_{x'x'} - \sigma_{xx'}^2 \ , \tag{5.1}$$

where

$$\sigma_{xx} = \frac{1}{Q}\sum_i^M Q_i(\sigma_{xxi} + (x_i - \bar{x})^2) \ , \tag{5.2}$$

Q is the total charge, M is the number of slices in the bunch, σ_{xxi} is the square of the standard deviation and x_i is the center in x of slice i, and the centroid of the bunch $\bar{x}$ is given by

$$\bar{x} = \frac{1}{Q}\sum_i^M Q_i x_i \ . \tag{5.3}$$

The other total moments $\sigma_{x'x'}$ and $\sigma_{xx'}$ are defined in an analogous fashion.

The effective emittance ϵ_x is a measure of the effective area in phase space populated by all the bunch slices. This definition of emittance again suffers from the problem that tail particles at large amplitudes can dominate the results, overestimating their effect on beam quality. One should not take very large values of emittance growth seriously, other than to note that the emittance growth is very large.

We then define the emittance growth factor $\delta\epsilon_x$ from position 0 to position 1 in the linac as

$$\delta\epsilon_x = \frac{(\bar{\gamma}\epsilon_x)_1 - (\bar{\gamma}\epsilon_x)_0}{(\bar{\gamma}\epsilon_x)_0} , \tag{5.4}$$

where $\bar{\gamma}$ is the average energy of the bunch. Normally position 0 is taken to be the beginning and position 1 the end of the linac.

What is normally called beam break-up is the misalignment of the slice centroids in phase space due to the action of the dipole wakefield. When there is an energy variation along the bunch the slices will twist with respect to each other, also contributing to emittance growth, but normally to a much lesser extent. This might be called a chromatic emittance growth.

5.2 Inducing an Energy Spread

The layout of one cell of the SLAC linac, sectors 2-30 is shown schematically in Fig. 18. Four cells followed by a drift of 2.5 m make up one 100 meter sector. The peak accelerating gradient is 18 MeV/m. To induce an energy spread in the beam we separate the 232 klystrons (one for each 12 meter accelerator section) into two families. Family a contains n_a klystrons phased so that the bunch center sits at phase ϕ_a with respect to the RF crest. In family b, containing the remaining klystrons, the bunch sits at phase ϕ_b. In the SLC without Landau damping, for minimal energy spread at the end of the linac, the bunch needs to sit at 12° ahead of the RF crest, to compensate the variation of the longitudinal wakefield along the bunch (see Chapter 3). With Landau damping, the bunch needs to see, on average, the same slope of the RF wave. Therefore, since all the accelerator sections are of the same length, we want

$$n_a \sin\phi_a + (232 - n_a)\sin\phi_b = 232 \sin 12^\circ . \tag{5.5}$$

The discrete focusing code LTRACK was used for the simulations. In all runs presented here the longitudinal distribution of the bunch is taken to be gaussian, truncated from $4\sigma_z$ in front of bunch center to $2\sigma_z$ behind, and with σ_z = 1mm. The number of particles contained in a bunch is 5×10^{10}. The number of slices is 16. The initial normalized emittance is $\gamma\epsilon_x = 3.0 \times 10^{-5}$rm. All slices begin upright, with $\sigma_{x0} = 300\mu$m, $\sigma_{x'0} = 42\mu$r and energy $E_0 =$

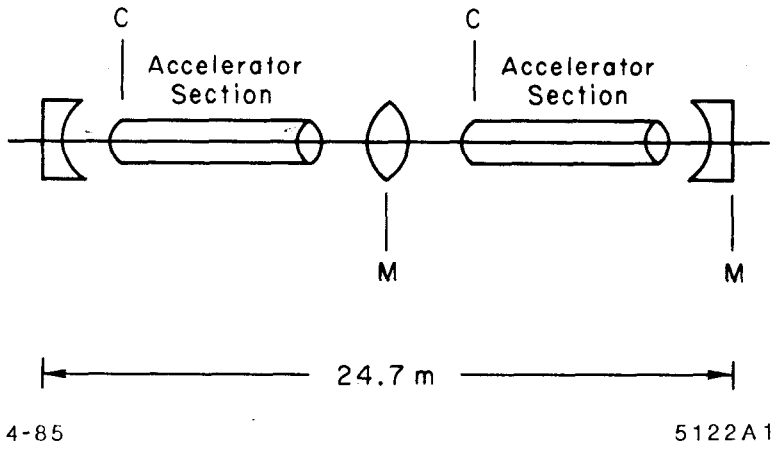

Fig. 18. One cell of the SLAC linac, sectors 2-30.

1.21GeV. In all runs the quads are adjusted such that the β-function of the central slice is matched, and as given in Fig. 19. For the first 1300 m the phase advance per cell is 90°. From there to the end of the linac the quad strengths are approximately equal to 110 kilogauss, their maximal value. The longitudinal and dipole wakefields of the average SLAC cell were used in the simulations of this chapter (see the solid curves of Figs. 2 and 3).

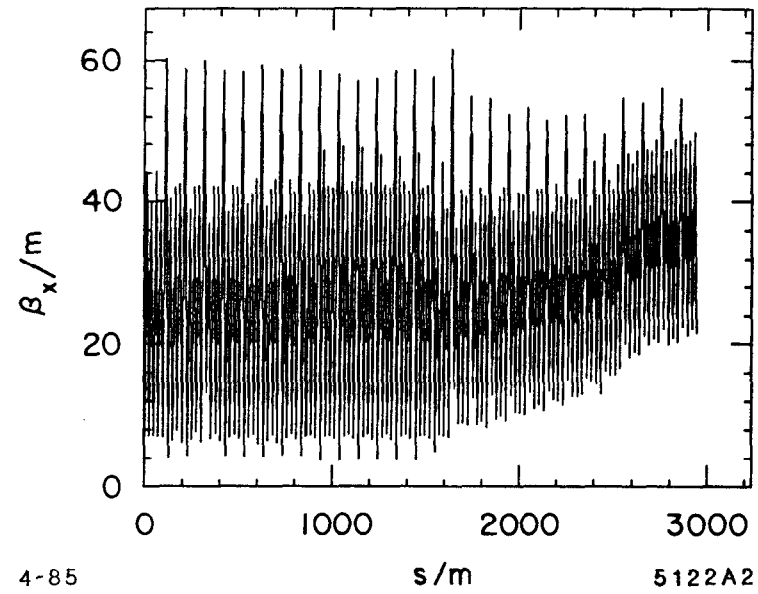

Fig. 19. The matched β-function in sectors 2-30.

5.3 THE IDEAL MACHINE

The LTRACK results for the SLAC linac with no errors are given in Fig. 20. Cases with $\phi_a = -15°, -30°, -45°, -60°$ were run. Fig. 20a gives the initial x offset that produces 25% emittance growth in the linac, x_d. The number n_a was adjusted in each case to maximize x_d. For the case with no Landau damping (denoted by NL in Fig. 20) we get $x_d = 2.1\mu$m. Fig. 20b gives the final energy E_F of the beam for the same runs. For no Landau damping $E_F = 50.0$GeV. The dashed curve gives E_F if we allow x_d to decrease by 20% from the optimal values, by reducing n_a, and gives an indication of the width of the minimum as a function of energy. We see that although we have more stability as ϕ_a becomes more negative (up to $\phi_a \approx -50°$) we lose more energy. The drop in x_d for $\phi_a < -50°$ is due to increased mismatch along the bunch (see below).

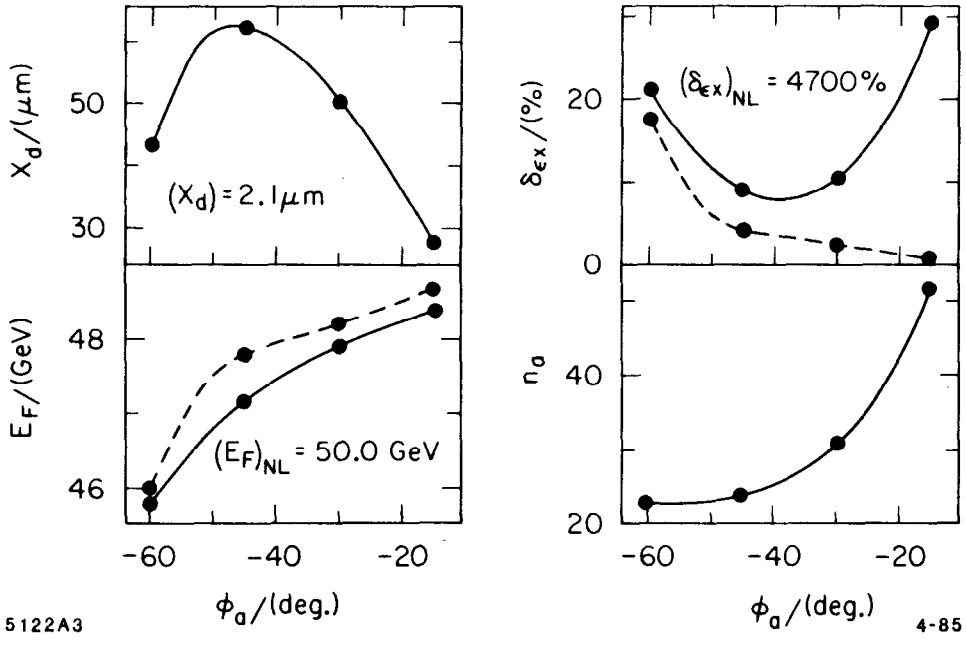

Fig. 20. Results for the error-free machine.

Fig. 20c gives the emittance growth for an initial offset $x_0 = 0.1\sigma_{x0} = 30\mu$m. For no Landau damping the emittance growth is very large. The dashed curve is the emittance growth for a beam launched on axis, and is due only to the twisting of the slices with respect to one another in phase space. This effect is stronger for ϕ_a more negative, and is in fact the dominant effect for $\phi_a = -60°$. This is due to the greater lattice mismatch along the bunch when the energy spread is added quickly rather than more gradually along the linac. Fig. 20d gives the values of n_a used.

In Fig. 21 the beam behavior with no Landau damping (column 1) is compared with the case where $\phi_a = -30°$ and $n_a = 31$ (column 2). The initial offset x_0 is 30μm. The bunch centroid $\bar{x}$ is plotted as a function of s in Fig. 21a, for the case with no damping. In Fig. 21b we see the rapid emittance growth along the linac. A scatter plot of the beam at the end of the linac is given in Fig. 21c. (The head is to the right.) Note that the tail half of the bunch is strongly perturbed; in comparison, the front half is little affected. For the case with damping, the oscillation amplitude first grows but then becomes quite small by the end of the linac (see Fig. 21d). A coherent emittance growth is induced early in the linac, which then largely disappears toward the end of the machine, as is seen in Fig. 21e. The beam arrives at the end of the linac relatively unperturbed, as shown in Fig. 21d.

5.4 The Machine With Errors

In order to study the effects of machine errors, runs with 100μm rms quadrupole offset errors (the SLC spec[16]) were done. Table 2 gives the results. Case 12 is with no Landau damping. In case 15 $\phi_a = -15°$ and $n_a = 51$; in case 30 $\phi_a = -30°$ and $n_a = 31$. The letters A-E represent four different sets of random numbers. First, correctors (C) were adjusted to correct a low current beam to beam position monitors (M) with 100μm rms offset errors (see Fig. 18). Then the high current beam was launched on axis with these same corrector settings. In this way the head of the beam was corrected to the monitors. (Correcting the high current beam directly does not work due to the large tail that is formed on the uncorrected beam with the level of errors studied here.) Column 2 gives the resultant emittance growth. The emittance growth at this point is much larger without than with Landau damping. By adjusting x_0 and x_0' coherent effects of the errors can be largely compensated (column 3). (In practice a screen monitor at the end of the linac would be used for the feedback in this procedure.) Note that the compensation is not perfect. In some cases the injection conditions have not enough leverage to reduce the final emittance to a small value. Note also that at this point Landau damping usually but not always results in a lower emittance growth than with no damping.

By now adjusting two correctors which are 90° apart at the beginning of sector 6, we can reduce the emittance further (column 4). (In practice the screen monitor would again be used here.) At this point $\delta_{\epsilon x}$ is no bigger than 30% in all the Landau damped cases. With no Landau damping the extra correction has little effect. The final column gives the minimal change in x_0 that increases the emittance by 25% above the values given in column 4, Δx_d. (Normally the effect is not the same for equal changes in the two directions.) The results agree well with those for the error-free machine, ranging from 70-100% of the values given in Fig. 20a. These runs are a sort of proof of principle indicating that the dispersive effects are manageable, at least for ϕ_a down to $-30°$.

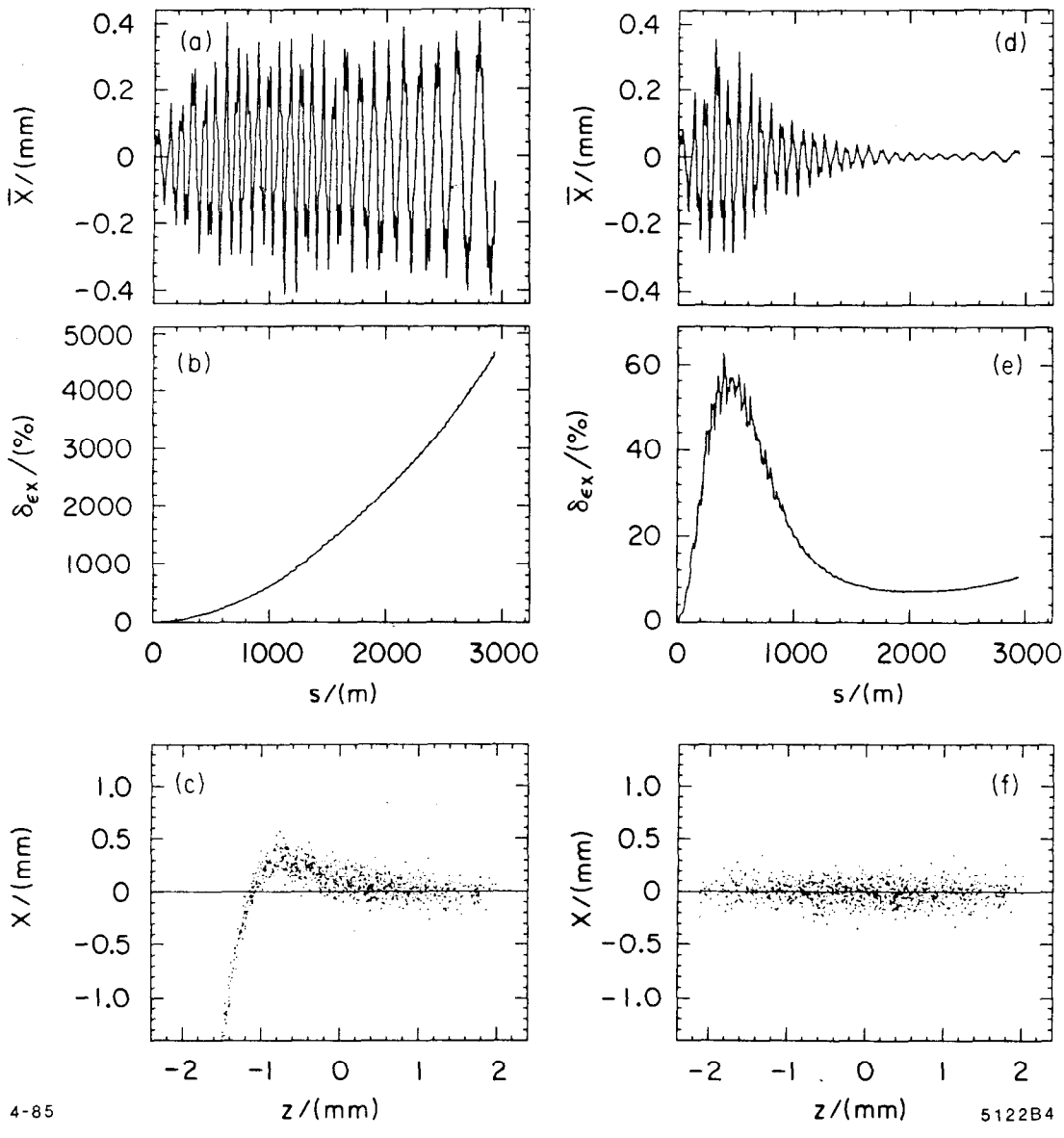

Fig. 21. Results without/with Landau damping.

5.5 CONCLUSIONS

In the SLC Landau damping can greatly stabilize the beam against changes in injection conditions into the linac. For example, by choosing $\phi_a = -15°$, $n_a = 51$, the jitter tolerances for 25% emittance growth can be relaxed by greater than a factor of 10, while sacrificing 1.6 GeV in final energy. Increasing the focusing, especially near the beginning of the linac, will lessen the energy penalty for a given amount of stability. For example, with the addition of more quads in sectors 2-4[31] the stability of the above example can be achieved at the cost of only 1.0 GeV in final energy. The simulations including machine errors indicate that the static residual emittance growth can be kept consistently below

Case	$(\delta_{\epsilon x})_a/\%$	$(\delta_{\epsilon x})_b/\%$	$(\delta_{\epsilon x})_c/\%$	$\Delta x_d/\mu$m
12A	944.	69.0	64.4	1.5
12B	1010.	39.9	37.5	1.8
12C	8150.	32.4	30.1	1.7
12D	3870.	404.2	374.6	2.6
12E	5080.	115.9	105.5	2.0
15A	271.	38.9	25.1	20.
15B	112.	10.3	6.9	24.
15C	82.	4.5	3.6	23.
15D	51.	16.7	11.4	20.
15E	332.	48.2	30.1	25.
30A	305.	126.2	23.5	36.
30B	92.	33.9	10.8	42.
30C	22.	6.0	4.7	51.
30D	138.	62.6	29.0	33.
30E	266.	96.1	18.7	39.

Table 2. Results for the machine with errors.

30% with Landau damping, but that this would be difficult to achieve without Landau damping.

Some Landau Damping simulation results for the SLC with the additional quads in sectors 2-4, is given in Ref. 17.

ACKNOWLEDGEMENTS

The author would like to thank P. Morton, A. Novokhatsky and M. Sands for helpful discussions. Thanks are due also to P. Wilson for reading the manuscript and for making a number of useful suggestions.

REFERENCES

1. V. Balakin, A. Novokhatsky, V. Smirnov, Proceedings of the 12th Int. Conf. on High Energy Accelerators Fermilab, (1983), p. 119.
2. V. Balakin and A. Novokhatsky, "Beam Dynamics in the VLEPP Linear Accelerator", International Conference of High Energy Accelerators, Novosibirsk (1986).
3. K. Bane, T. Weiland, P. Wilson, in *Physics of High Energy Particle Accelerators*, AIP Conf. Proc. No. 127, (Am. Inst. of Physics, New York, 1983), Chapter 2.
4. K. Bane and P. Wilson, Proceedings of the 11th Int. Conf. on High-Energy Accelerators, CERN (Birkhäuser Verlag,Basel,1980),p. 592.
5. K. Bane, CERN/ISR-TH/80-47 (1980).
6. W. Panofsky and W. Wenzel, *Rev. Sci. Instrum.* **27**, 967 (1956).
7. T. Weiland, DESY M83-02 (1983) and *Nucl. Instr. Meth.* **216**, 31 (1983).
8. T. Weiland, DESY **82**-015 (1982) and *Nucl. Instr. Meth.* **212**, 13 (1983).
9. A. Novokhatsky, Novosibirsk Preprint 82-157 (1982).
10. P. Wilson in *Physics of High Energy Particle Accelerators*, AIP Conf. Proc. No. 87, (Am. Inst. of Physics, New York, 1982), Sec. 11.1.
11. A. Chao in *Physics of High Energy Particle Accelerators*, AIP Conf. Proc. No. 105, (Am. Inst. of Physics, New York, 1983), Sec. 2.3.
12. E. Keil, *Nucl. Instr. Meth.* **100**, 419 (1972).
13. D. Brandt and B. Zotter, CERN-ISR/TH/82-13 and LEP Note 388 (1982).
14. D. Brandt, CERN-LEP Note 484 (1984).
15. K. Bane and B. Zotter, Proceedings of the 11th Int. Conf. on High Energy Accelerators, CERN (Birkhäuser Verlag, Basel,1980), p. 581.
16. SLC Design Handbook, SLAC (1984).
17. J. Seeman and J. Sheppard, "Special SLC Linac Developments", 1986 Linear Accelerator Conference, SLAC and SLAC-PUB-3944 (1986).
18. G. Loew and J. Wang, *IEEE Trans. Nucl. Sci.* **NS-32**, 3228 (1985).
19. V. Balakin and A. Novokhatsky, Proceedings of the 12th Int. Conf. on High Energy Accelerators Fermilab, (1983), p. 117.
20. P. Wilson, "Future e^+e^- Linear Colliders and Beam-Beam Effects", 1986 Linear Accelerator Conference, SLAC and SLAC-PUB-3985 (1986).

21. H. Henke and W. Schnell, CERN-LEP-RF/86-18 and CLIC Note 22 (1986).

22. A. Chao, B. Richter, C. Yao, *Nucl. Instr. Meth.* **178**, 1 (1980).

23. Y. Chin, CERN-SPS/86-05 (1986).

24. K. Yokoya, DESY **86**-084, Appendix A (1986).

25. F. Selph and A. Sessler, LBL-20083 (1985) and *Nucl. Instr. Meth.* **A244**, 323 (1986).

26. A. Mondelli *et. al.*, "Frequency Scaling of Linear Super-Colliders", 1986 Linear Accelerator Conference, SLAC (1986).

27. H. Henke, private communication.

28. A. Chao and R. Cooper, *Particle Accelerators* **13**, 1 (1983).

29. K. Brown, *Advances Particle Phys.* **1**, 71-134 (1967).

30. K. Bane, *IEEE Trans. Nucl. Sci.* **NS-32**, 2389 (1985).

31. J. Seeman, *et. al. IEEE Trans. Nucl. Sci.* **NS-32**, 1662 (1985).